Session 4: Planetary atmospheres

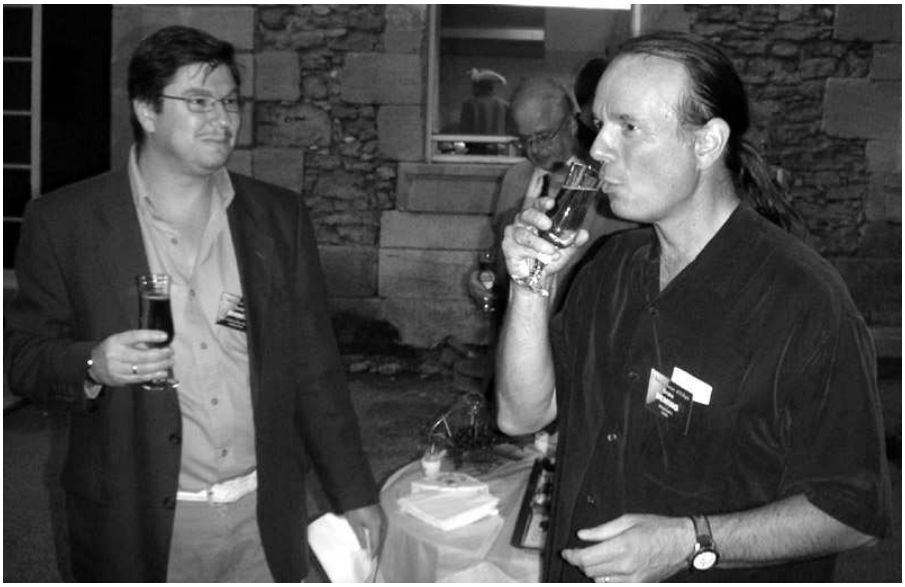

Tenth anniversary of 51 Peg-b : Status of and prospects for hot Jupiter studies
Proceedings of Haute Provence Observatory Colloquium (22-25 August 2005)
Edited by L. Arnold, F. Bouchy, and C. Moutou

The evolution and structure of Pegasi planets: ten years of models and still much to learn!

T. Guillot

Observatoire de la Côte d'Azur, CNRS UMR 6202, BP 4229, 06304 Nice Cedex 4, France [guillot@obs-nice.fr]

Abstract. Ten years after the discovery of 51 Peg b, our understanding of the evolution of "Pegasi planets" (a.k.a. "Hot Jupiters") has been shaken several times: by the discovery of the first transiting extrasolar planet, HD209458b and its large radius, the discovery of the evaporation of this planet, the measurement of the radii of several other extrasolar planets, and recently by measurements of the infrared planetary emission by the detection of the secondary eclipse for 2 Pegasides. I discuss the different theoretical explanations and models that have been proposed to explain the observations. Our understanding of Pegasides is far from complete, but great hope lies in statistical observations and characterization of transiting planets with ground based programs and the space missions COROT and Kepler.

1. Introduction

More than 150 extrasolar planets have been discovered to date (see J. Schneider's *Extrasolar Planets Encyclopedia* on http://www.obspm.fr/planets), but only those for which a determination of both the planetary mass and radius are useful for the purposes of this review. This can only be done for planets which transit in front of their star, which, by probabilistic arguments limits us to planets that orbit close to their star. I will therefore only be concerned with "Pegasi planets", giant planets similar to 51 Peg b and HD209458b (both in the constellation Pegasus), with semi-major axes smaller than 0.1 AU.

Nine transiting Pegasi planets have been discovered so far. The main characteristics of seven of them are listed in Table 1 (OGLE10 has been omitted because of uncertainties on the radius measurement, and HD189733 because it is too recent). The first one, HD209458b

(Charbonneau et al. 2000; Henry et al. 2000), has been shown to possess sodium in its atmosphere (Charbonneau et al. 2002) and to have an extended, evaporating atmosphere (Vidal-Madjar et al. 2003, 2004). Four others have been discovered by the photometric OGLE survey and subsequent radial velocity measurements (Konacki et al. 2003, 2004; Bouchy et al. 2004, Pont et al. 2004). One is a result of the TrES network survey (Alonso et al. 2004). Finally, HD149026 has been discovered by a dedicated high-metallicity radial-velocimetry survey (Sato et al. 2005). Present photometric surveys have a strong detection bias towards very short periods. Associated to a probability of transiting that is inversely proportional to the orbital distance, this shows that Table 1 represents only a tiny fraction of planets, which hence may have a low probability of existence.

Table 1. *Characteristics of 7 transiting Pegasi planets*

	Age [Ga]	[Fe/H]	$T^\star_{\rm eq}$ [K]	$M_{\rm p}/M_{\rm J}$	$R_{\rm p}/10^{10}$ cm
HD209458[a]	$4-7$	0.00(2)	1460(120)	0.69(2)	1.02(9)
OGLE-56[b]	$2-4$	0.0(3)	1990(140)	1.45(23)	0.88(11)
OGLE-113[c]	?	0.14(14)	1330(80)	1.35(22)	$0.77\binom{+5}{-4}$
OGLE-132[d]	$0-1.4$	0.43(18)	2110(150)	1.19(13)	0.81(6)
OGLE-111[e]	?	0.12(28)	1040(160)	0.53(11)	$0.71\binom{+9}{-4}$
TrES-1[f]	?	0.00(4)	1180(140)	0.75(7)	0.77(4)
HD149026[g]	$1.0-3.0$	0.36(5)	1740	0.33(3)	0.52(4)

* Equilibrium temperature calculated on the basis of a zero planetary albedo
[a]Cody & Sasselov (2002), Brown et al. (2001)
[b]Torres et al. (2004), Sasselov (2003), Konacki et al. (2003)
[c]Bouchy et al. (2004), Konacki et al. (2004)
[d]Moutou et al. (2004)
[e]Pont et al. (2004)
[f]Laughlin et al. (2005), Sozzetti et al. (2004), Alonso et al. (2004)
[g]Sato et al. (2005), Charbonneau et al. (2005)

A crucial parameter for the evolution models is the equilibrium temperature $T_{\rm eq} = T_*\sqrt{R_*/2a}$ (assuming a zero albedo, i.e. that all incoming stellar light is absorbed by the planetary atmosphere). With values of $T_{\rm eq}$ between ~ 1000 and 2000 K, the present sample of transiting planets is already quite rich.

In the next sections, I discuss how observed radii compare to theoretical calculations and derive constraints on the amount of heavy elements present in HD149026b. I then discuss several questions that directly impact our ability to understand and model the evolution of Pegasides.

2. Observed vs. calculated radii of Pegasi planets

Contrary to the giant planets in our Solar System, Pegasi planets are subject to an irradiation from their central star that is so intense that the absorbed stellar energy flux is about $\sim 10^4$ times larger than their intrinsic flux). The atmosphere is thus prevented from cooling, with the consequence that a radiative zone develops and governs the cooling and contraction of the interior (Guillot et al. 1996). Typically, for a planet like HD209458b, this radiative zone extends to kbar levels, $T \sim 4000\,\mathrm{K}$, and is located in the outer 5% in radius (0.3% in mass) (Guillot & Showman 2002).

Problems in the modeling of the evolution of Pegasi planets arise mostly because of the uncertain outer boundary condition. The intense stellar flux implies that the atmospheric temperature profile is extremely dependent upon the opacity sources considered. Depending on the chosen composition, the opacity data used, the assumed presence of clouds, the geometry considered, resulting temperatures in the deep atmosphere can differ by up to $\sim 600\,\mathrm{K}$ (Seager & Sasselov 1998, 2000; Goukenleuque et al. 2000; Barman et al. 2001; Sudarsky et al. 2003; Iro et al. 2005). Because of this problem, and in the framework of our simple model, the following discussion will be based on an outer boundary condition at 1 bar and a fixed temperature $T_1 = 1500$ or $2000\,\mathrm{K}$[1].

Another related problem is the presence of the radiative zone. Again, the composition is unknown and the opacity data are uncertain in this relatively high temperature ($T \sim 1500 - 3000\,\mathrm{K}$) and high pressure (up to $\sim 1\,\mathrm{kbar}$) regime. Results from our models are based on opacities from Allard et al. (2001). Other calculations using e.g. the widely used Alexander & Ferguson (1994) opacities do yield only a slightly faster cooling even though the Rosseland opacities are lower by a factor ~ 3 in this regime.

The resulting mass-radius relations are shown in Fig. 1 for $T_1 = 1500$ and 2000 K, and compared to the observations for the planets listed in Table 1. For each case, an upper limit on the radius is obtained from a pure hydrogen-helium composition with $Y = 0.25$. An ad hoc lower limit comes from a model with a $15\,\mathrm{M}_\oplus$ central core, and a $Y = 0.30$ envelope. In both case, the opacity table is unchanged.

---

[1] Technically, in order to obtain high entropy initial conditions I use $T_1 \approx T_{\rm eq}(1 + L/L_{\rm eq})^{1/4}$, but the precise form does not matter as long as $L \ll L_{\rm eq}$, or equivalently $-T_1 dS_1/dt \ll -T_{\rm int} dS_{\rm int}/dt$ where $S_{\rm int}$ is the characteristic interior entropy. The equality between T_1 and $T_{\rm eq}$ is only a very rough estimate guided by present works on atmospheric models of heavily irradiated planets.

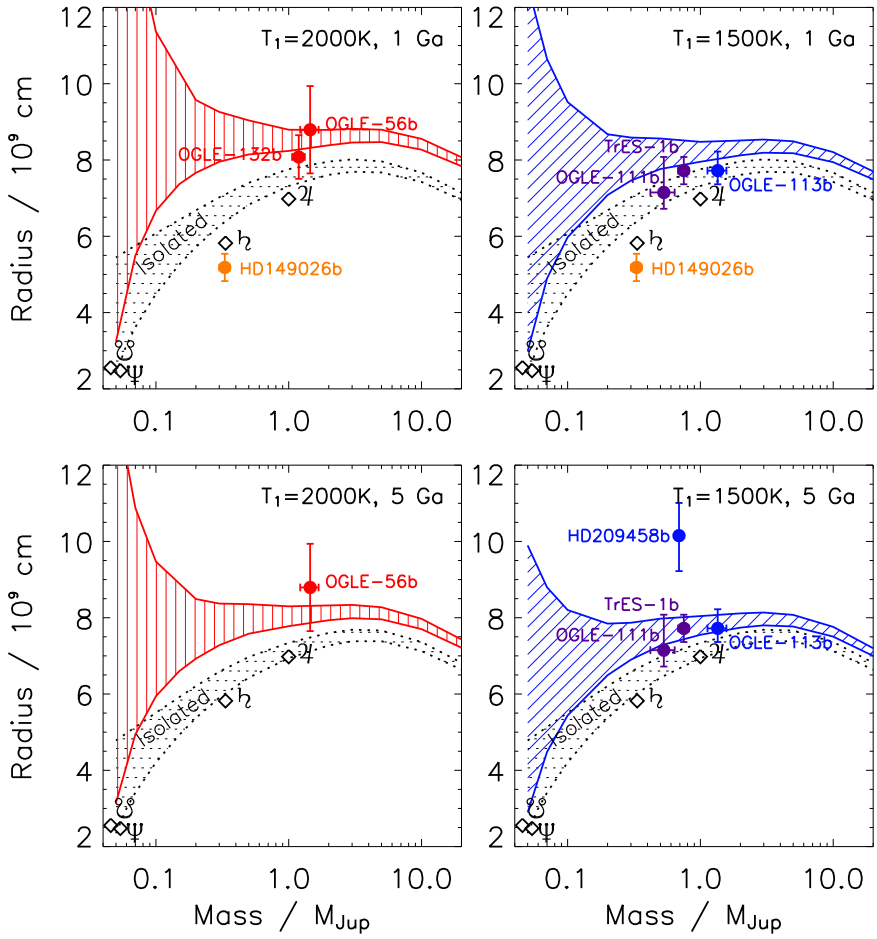

Figure 1. *Mass-radius relation of strongly irradiated planets with ages of 1 Ga (upper panels) and 5 Ga (lower panels), and 1-bar temperatures equal to 2000 (left panels) and 1500 K (right panets), respectively. The hashed areas have upper and lower envelopes defined by* ($Y = 0.25$, $M_{\rm core} = 0$) *and* ($Y = 0.30$, $M_{\rm core} = 15\,M_\oplus$), *respectively. Dotted symbols with error bars indicate known objects, plotted as a function of their estimated 1-bar temperatures and ages. Planets whose age is uncertain appear in both upper and lower panels. Results for non-irradiated planets (dotted lines) are shown for an easier comparison. [Adapted from Guillot (2005)].*

Figure 1 shows that within uncertainties, the measurements for 4 planets out of 7 can be explained in the framework of our simple model. However, three cases stand out: OGLE-TR-132b appears too small for its age implying that it may contain significant amounts of heavy elements in a core or in its deep interior. HD149026b is more obvious and requires the presence of a large mass of heavy elements in its interior, as discussed in the next section. The case of HD209458b is more problematic: the constraints on its age, mass, an deep atmospheric temperature that should be $\sim 1500 - 2000$ K yield radii that are about 10 to 20% smaller than measured (Bodenheimer et al. 2001; Guillot & Showman 2002; Baraffe et al. 2003). The fact that the measured radius corresponds to a low-pressure ($\sim$mbar) level while the calculated radius corresponds to a level near 1 bar is not negligible (Burrows et al. 2004) but too small to account for the difference. This is problematic because while it is easy to invoke the presence of a massive core to explain the small size of a planet, a large size such as that of HD209458b may require an additional energy source.

Bodenheimer et al. (2001) proposed that this large radius may be due to a small forced eccentricity ($e \sim 0.03$) of HD209458b, and subsequent tidal dissipation in the planet interior. This explanation requires the presence of an unseen companion. Furthermore, Spitzer observations showing that the primary and secondary eclipses occur at equidistant time intervals (within the error bars), imply that the probability for the orbit to be eccentric is low (Deming et al. 2005).

A natural possibility may be the stellar flux itself, since transporting to deep levels (~ 100 bars or more) only a small fraction of order 0.1% to 1% of the incoming flux would yield a radius that is in agreement with the observations. On this basis, Showman & Guillot (2002) proposed that kinetic energy generated in the atmosphere due to the strong asymmetry in stellar insolation may be transported to deep levels and dissipated there, possibly due to a small asynchronous rotation and its dissipation by stellar tides. Another possibility evoked by the authors that km/s atmospheric winds may maintain the atmosphere into a shear-unstable, quasi-adiabatic state, which would force temperatures in excess of 3000 K at levels between 10 and a few tens of bars.

It is puzzling that all other transiting planets from table 1 do not require an additional energy source to explain their size: this is seen in fig. 1, which shows that all planets except HD209458b are consistent with the evolutionary tracks.

Is there a consistent scenario explaining all the observations? A possibility is that their orbital histories have been very different. However, I would favor the possibility that the planets are all subject to some form of energy dissipation, but that they have very different compositions (and very different core masses) (see Guillot 2005).

3. The case of HD149026

Let us now describe the evolution of HD149026b because it is emblematic of the case for a strong variability of core masses and/or masses of heavy elements in Pegasi planets. Figure 2 indeed shows that, as discussed in the discovery paper by Sato et al. (2005), the small radius of the planet can only be explained through the existence of a large amount of heavy elements, between 45 and 80 $M_\oplus$, present inside the planet.

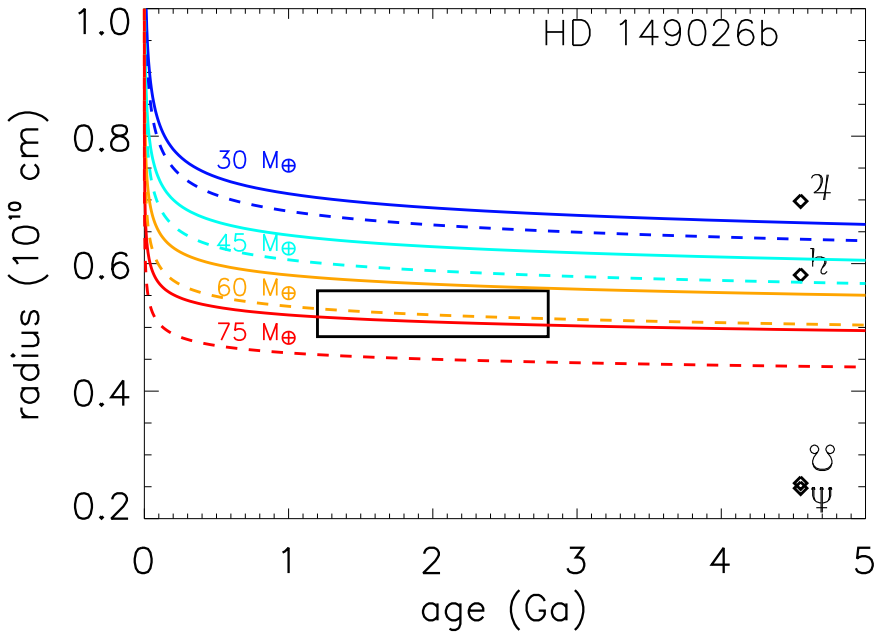

Figure 2. *Evolution of the radius of a 0.36 $M_{\rm Jup}$ planet made of a central core of 30 to 75 $M_\oplus$ and a gaseous envelope of solar composition. The planet is irradiated so that $T_{\rm eq} = 1740$ K (see text). The core is assumed to be made of ices (plain lines) or rocks (dashed lines). The results are compared to the observations for HD149026b (black box).*

The fact that the star HD149026 is highly metal-rich also strengthens the link between metallicity and large amounts of heavy elements present in the planet. This implies that, whatever the formation process was, metallicity played a key role in the formation of giant planets.

4. How do tides and orbital evolution affect the contraction and cooling of Pegasi planets?

The small orbital eccentricities of Pegasi planets compared to more distant extrasolar planets tells us that tides raised by the star on the planet have probably played an important role in circularizing their orbits, with a timescale estimated at $\sim 1\,\mathrm{Ga}$ for a planet at 0.05 AU (Rasio et al. 1996; Marcy et al. 1997). Synchronization is expected to occur in only Ma timescales (Guillot et al. 1996), maybe much less (Lubow et al. 1997). The tides raised by the planet on the star also tend to spin up the star which leads to a decay of the planetary orbit. It is interesting to note that, with periods of only $\sim 1\,\mathrm{day}$ the three OGLE planets lie close to the orbital stability threshold (Rasio et al. 1996), or would be predicted to fall into the star in Ga timescales or less (Witte & Savonije 2002; Pätzold & Rauer 2002).

The energies available from circularisation and synchronization can be usefully compared to the gravitational energy of the planet (e.g. Bodenheimer et al. 2001; Showman & Guillot 2002): they are of order 4×10^{42} erg, 2×10^{41} erg and 2×10^{42} erg for "typical" Pegasi planets with a $1\,\mathrm{M_J}$ mass assuming a 0.1 eccentricity (see Guillot 2005 for details).

The fact that the three energy sources are comparable imply that very early in the evolution, circularisation and synchronization may have played a role, perhaps inducing mass loss (Gu et al. 2004). Once a planet has contracted to a degenerate, low θ state, the gravitational energy becomes large, and circularisation and synchronization only have a limited role to play. However, two reservoirs can be invoked: the orbital energy of a massive eccentric planet that would force a non-zero eccentricity of the inner one (Bodenheimer et al. 2001) and the absorbed stellar luminosity in its ability to create kinetic energy in the atmosphere (Showman & Guillot 2002).

A major uncertainty related to these processes and how they affect the planetary structure is to know how and where energy is dissipated. Lubow et al. (1997) proposed that a resonant tidal torque is exerted at the outer boundary of the inner convection zone, and that dissipation occurs through the damping of gravity waves propagating in the outer stable radiative region. Contrary to Jupiter, this may be an efficient process because Pegasi planets have a radiative region that extends to great depths. Another possibility is through the excitation of inertial waves in the convective region, a process that would occur also in our giant planets (Ogilvie & Lin 2004). The location of the dissipation is not clear, however. If it occurs in the atmosphere, the effect of tides on the evolution will be limited, whereas they will have a maximum impact if they occur deep into the radiative zone (Guillot & Showman 2002).

If dissipation cannot reach into the deep interior, the planets will not inflate significantly when they migrate to their present location. This would imply that HD209458b must have migrated from several AUs to its present location in less than ~ 10 Ma (Burrows et al. 2000b). In this framework, one could invoke a late migration of the OGLE planets (in particular OGLE-TR-132b) to explain their relatively small radius compared to HD209458b.

5. How does the composition affects the structure and evolution?

It is generally believed that giant planets of the mass of Jupiter should have near solar composition and relatively small core masses. However, it may not be the case: first, Jupiter is in fact relatively significantly enriched in heavy elements. Second, while Jupiter is very efficient at ejecting planetesimals from the Solar System, Pegasi planets are unable to do so because the local orbital speed $(GM_*/a)^{1/2} \sim 150\,\mathrm{km\,s^{-1}}$ is much larger than the planet's escape velocity $(2GM/R)^{1/2} \sim 50\,\mathrm{km\,s^{-1}}$ (Guillot & Gladman 2000). Furthermore, most planetesimals on low e orbits close to the planet would end up impacting the planet, not the star (A. Morbidelli, pers. communication 2004). Pegasi planets should therefore be expected to have very different compositions and core masses, depending on the properties of the disk of planetesimals at their formation, the presence of other planets, and their orbital evolution.

The presence of a core has a relatively straightforward impact on the evolution of giants planets. As shown in fig. 1, it leads to a much faster contraction and a smaller radius at any given age. An enrichment of the envelope both increases the mean molecular weight and the opacities, with two opposite effects in terms of the planet's contraction and cooling. Figure 3 shows that for large irradiations (extended radiative zones), the second effect wins and leads to a (limited) increase of the planetary radius. However, planets with a larger mean molecular weight eventually become smaller.

The difference in inferred radii between HD209458b and other transiting planets could hence indicate that stellar tides play a role in slowing or even stalling the contraction of all planets, but that because of different histories, some planets have a large core mass but HD209458b has not. In that framework, OGLE-TR-132b would probably need a core of ~ 20 $M_\oplus$ or more (or the same amount of heavy elements in its deep interior) to explain its small radius. The large [Fe/H] value measured for its parent star (Table 1) is an indication that the planet may indeed have grown a large core.

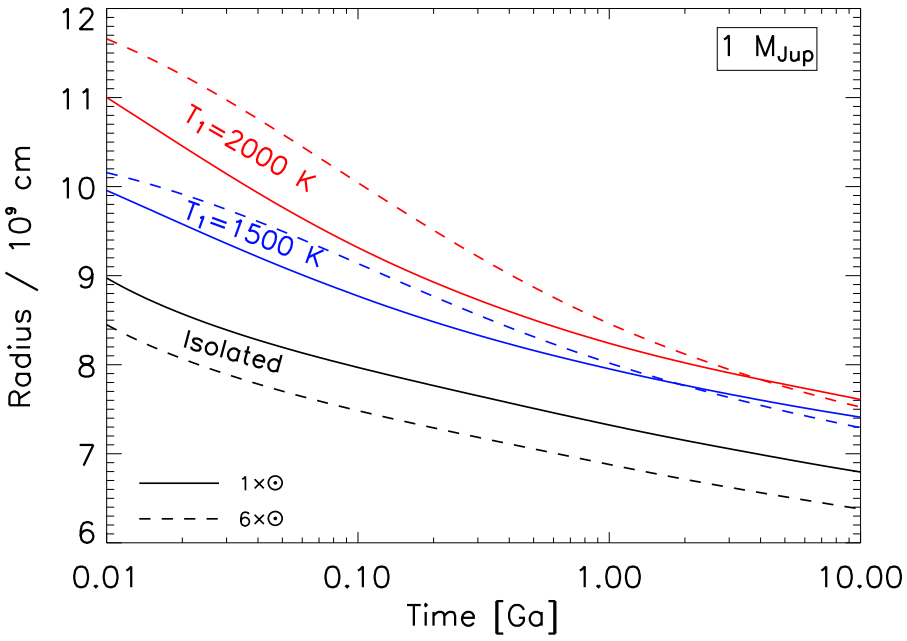

Figure 3. *Evolution of giant planets in terms of radius vs. time, for different irradiation levels, and 2 assumed compositions: 1 and 6 times solar. (This calculation ignores 2nd order effects as modifications of the adiabatic temperature gradient and non-linear effects in the opacity calculation, and more importantly modifications of atmospheric properties.). [From Guillot 2005].*

6. What is the role of the atmosphere for the evolution?

I have purposely used a very simple atmospheric model by setting $T_1 \propto T_{\rm eq} = $ cte. Of course, this hides many important complications like opacities, chemistry, gravity dependence, presence of clouds, atmospheric dynamics, dependence on the incoming stellar flux...etc. These complications partially explain differences between several authors (Seager & Sasselov 1998, 2000; Goukenleuque et al. 2000; Barman et al. 2001; Sudarsky et al. 2003; Iro et al. 2005). These works yield characteristic temperatures at the base of the atmosphere (i.e. where most of the incoming flux has been absorbed) that range from $\sim$ 1700 to $\sim$ 2300 K.

However, the largest differences arise from simple geometrical reasons: Because these calculations are one-dimensional, some authors

choose to model the atmosphere at the substellar point, some average the received stellar flux over the day-hemisphere (1/2 less flux), and others average it over the entire planet (1/4 less flux). This points to real problems: how does the planet reacts to this extremely inhomogeneous stellar irradiation, and how do possible inhomogeneities in the atmosphere affect the planetary evolution?

Without atmospheric dynamics, a synchronous Pegasi planet at $\sim$ 0.05 AU of a G-type star would see its substellar point heated to $\sim$ 2500 K or more, and its night hemisphere and poles have temperatures $\sim$ 100 K, a clearly unstable situation. Assuming synchronization of the convective interior and a radiative atmosphere obeying the Richardson shear-instability criterion, Showman & Guillot (2002) showed that the atmosphere of Pegasi planets are likely to develop km/s winds, but that spatial photospheric temperature variations of $\sim$ 500 K are likely. Dynamical models using shallow-water equations by Cho et al. (2003) also yield latitudinal temperature variations, but predict a surprising time-dependent behavior, with a night-side that sometimes becomes hotter than the day side. A time-Dependant approach of radiative transfer, in which the atmosphere is allowed to react to a varying irradiation, shows that a km/s rotation indeed yields a $\sim$ 500 K effective temperature variation. It also shows that the conditions required for the shallow-water treatment (a relatively long radiative timescale) are probably not met in Pegasi planets (Iro et al. 2005).

As shown by Guillot & Showman (2002), to first order (i.e. neglecting possible non-linear behavior due to e.g. opacity temperature dependences and/or cloud formation), the cooling with an inhomogeneous boundary condition is faster than if the same amount of heat has been homogeneous distributed. This is because heat tends to escape more rapidly in regions of low atmospheric temperatures. But since the radiative timescale below optical depth unity is approximatively $\propto P^2$, levels deeper than a few bars tend to homogenize horizontally very efficiently, even with a slow circulation (Iro et al. 2005).

Therefore, there is presently no reason to use for evolution models an atmospheric boundary condition other than that obtained assuming a stellar flux averaged over the entire planet. Of course, more work is to be done, as opacity variations, the presence of clouds either on the day or night side (depending on the kind of circulation), non-equilibrium chemistry, and possible shear instabilities and gravity waves damping can all play an important role.

7. Stability and evaporation?

Because Pegasi planets are so close to their star, the question of their survival has been among the first following the discovery of 51 Peg B. Guillot et al. (1996) and Lin et al. (1996) independently concluded to a relatively fast contraction of the planet and to its survival based on non-thermal evaporation rates extrapolated from Jupiter. These evaporation rates $\sim 10^{-16}\,M_\odot\,a^{-1}$ turn out to be extremely close to those inferred from observations of HD209458b showing the escape of HI (Vidal-Madjar et al. 2003), OI and CII (Vidal-Madjar et al. 2004). However, the atmospheric escape problem is more complex than initially envisioned, with XUV heating, conduction and gravity waves playing important roles (Lammer et al. 2003; Lecavelier des Etangs et al. 2004).

Generally, a critical question is that of the stability of planets at close orbital distances in their young ages (Baraffe et al. 2004; Gu et al. 2004). Figure 3 shows that the cooling timescale is initially relatively long in the case of intense irradiation (see also fig. 2 of Guillot et al. 1996) and might lead to a significant mass loss in case of a rapid inward migration because of Roche lobe overflow (part of the planetary envelope becomes unbound because of the star's gravitational potential) (Trilling et al. 1998, 2002). Baraffe et al. (2004) find that another route may be the strong exospheric evaporation. Below a critical mass, the planet would inflate before it can become degenerate enough. However, either the presence of a core and the consequent rapid contraction (see fig. 1), or an internal cooling associated to the decompression upon mass loss may protect the planets from an exponential evaporation.

8. Conclusion & prospects

We are just beginning to discover the diversity of giant planets. Already, a variety of problems that are particular to one planet or a small ensemble of planets have arisen. Given the limited ensemble of objects that we are given to study and the rapid evolution of the subject, any attempt to find general rules it fraught with risk. It seems safe to assert that, like Jupiter and Saturn, the Pegasi planets discovered so far are mostly made of hydrogen and helium, but their precise composition depends on how tidal effects lead to the dissipation of heat in their interior. In some cases (HD149026b in particular), hydrogen and helium may well represent less than half of the total planetary mass.

Improvements on our knowledge of the giant planets requires a variety of efforts that include obtaining better high pressure equations of state experimentally and numerically, probing with dedicated space missions our own giants, Jupiter, Saturn, Uranus and Neptune, and

making progresses on the detection and characterization of extrasolar planets. Fortunately, nearly all of these are addressed at least partially by adequate projects in the next few years. Most importantly, the space missions COROT (2006) and *Kepler* (2007) should provide the detection and characterization of many tens, possibly hundreds of giant planets and allow reliable statistical tests to understand what Pegasides are made of and how they were formed.

Clearly, there is a lot of work on the road, but the prospects for a much improved knowledge of giant planets and their formation are bright.

References

Alexander, D.R. & Ferguson, J.W., 1994, ApJ, 437, 879

Allard, F., Hauschildt, P.H., Alexander D.R., *et al.*, 2001, ApJ, 556, 357

Alonso, R., Brown, T.M., Torres, G., *et al.*, 2004, ApJ, 613, L153

Baraffe, I., Chabrier, G., Barman, T.S., *et al.*, 2003, A&A, 402, 701

Baraffe, I., Selsis, F., Chabrier, G., *et al.*, 2004, A&A, 419, L13

Barman, T., Hauschildt, P.H., Allard, F., 2001, ApJ, 556, 885

Bodenheimer, P., Lin, D.N.C., Mardling, R., 2001, ApJ, 548, 466

Bouchy, F., Pont, F., Santos, N.C., *et al.*, 2004, A&A, 421, L13

Brown, T.M., Charbonneau, D., Gilliland, R.L., *et al.*, 2001, ApJ, 552, 699

Burrows, A., Marley, MS. & Sharp, C.M., 2000a, ApJ, 531, 438

Burrows, A., Guillot, T., Hubbard, W.B., *et al.*, 2000b, ApJL, 534, L97

Burrows, A., Hubeny, I., Hubbard, W.B., *et al.*, 2004, ApJ, 610, L53

Charbonneau, D., Brown, T.M., Latham, D.W., *et al.*, 2000, ApJ, 529, L45

Charbonneau, D., Brown, T.M., Noyes, R.W., *et al.*, 2002, ApJ, 568, 377

Charbonneau D et al., 2005, submitted to ApJ [astro-ph/0508051]

Cho, J.Y.K., Menou, K., Hansen, B.M.S., *et al.*, 2003, ApJ, 587, L117

Cody, A.M. & Sasselov, D.D., 2002, ApJ, 569, 451

Goukenleuque, C., Bézard, B., Joguet, B., *et al.*, 2000, Icarus, 143, 308

Gu, P.G., Bodenheimer, P.H., Lin, D.N.C., 2004, ApJ, 608, 1076

Guillot, T., Burrows, A., Hubbard, W.B., *et al.*, 1996, ApJ, 459, L35

Guillot, T., 2005, Ann. Rev. Earth & Plan. Sci., 33, 493

Guillot, T., & Gladman, B., 2000, in *Proceedings of the Disks, Planetesimals and Planets Conference, ASP Conference Series*, eds F Garzon et al., 219, 475

Guillot, T. & Showman, A., 2002, A&A, 385, 156

Henry, G.W., Marcy, G.W., Butler, R.P., *et al.*, 2000, ApJ, 529, L41

Iro, N., Bézard, B., Guillot, T., 2005, A&A, 436, 719

Konacki, M., Torres, G., Jha, S., *et al.*, 2003, Nature, 421, 507

Konacki, M., Torres, G., Sasselov, D.D., *et al.*, 2004, ApJ, 609, L37

Lammer, H., Selsis, F., Ribas, I., *et al.*, 2003, ApJ, 598, L121

Laughlin, G., Wolf, A., Vanmunster, T., *et al.*, 2005, ApJ, 621, 1072

Lecavelier des Etangs, A., Vidal-Madjar, A., McConnell, J.C., *et al.*, 2004, A&A, 418, L1

Levison, H.F. & Morbidelli, A., 2003, Nature, 426, 419

Lin, D.N.C., Bodenheimer, P., & Richardson, D.C., 1996, Nature, 380, 606

Lubow SH, Tout CA & Livio M, 1997, ApJ, 484, 866

Marcy, G.W., Butler, R.P., Williams, E., *et al.*, 1997, ApJ, 481, 926

Moutou, C., Pont, F., Bouchy, F. *et al.*, A&A, 424, L31

Ogilvie, G.I., Lin, D.N.C., 2004, ApJ, 610, 477

Pätzold, M., Rauer, H., 2002, ApJ, 568, L117

Pont, F., Bouchy, F., Queloz, D., *et al.*, 2004, A&A, 426, L15

Rasio, F., Tout, C.A., Lubow, S.H., Livio, M., 1996, ApJ, 470, 1187

Sasselov, D.D., 2003, ApJ, 596, 1327

Sato, B. *et al.*, 2005, ApJ, 633, 465

Seager, S. & Sasselov, D.D., 1998, ApJ, 502, L157

Seager, S. & Sasselov, D.D., 2000., ApJ, 537, 916

Showman, A.P. & Guillot, T., 2002, A&A, 385, 166

Sozzetti, A., Young, D., Torres, G., *et al.*, 2004, ApJL, 616, L167

Sudarsky, D., Burrows, A. & Hubeny, I., 2003, ApJ, 588, 1121

Torres, G., Konacki, M., Sasselov, D.D., *et al.*, 2004, ApJ, 609, 1071

Trilling, D.E., Benz, W., Guillot, T., *et al.*, 1998, ApJ, 500, 428

Trilling, D.E., Lunine, J.I. & Benz, W., 2002, A&A, 394, 241

Vidal-Madjar, A., Désert, J.-M., Lecavelier des Etangs, A., *et al.*, 2004, ApJ, 604, L69

Vidal-Madjar, A., Lecavelier des Etangs, A., Désert, J.-M., *et al.*, 2003, Nature, 422, 143

Witte, M.G., Savonije, G.J., 2002, A&A, 386, 222

Tenth anniversary of 51 Peg-b : Status of and prospects for hot Jupiter studies
Proceedings of Haute Provence Observatory Colloquium (22-25 August 2005)
Edited by L. Arnold, F. Bouchy, and C. Moutou

Infrared radiation from hot Jupiters

D. Deming[1], L.J. Richardson[2], S. Seager[3], and J. Harrington[4]

[1]*Planetary Systems Laboratory, NASA's Goddard Space Flight Center, Code 693, Greenbelt, MD 20771 USA*
[ddeming@pop600.gsfc.nasa.gov]

[2]*NRC Research Associate in the Exoplanet and Stellar Astrophysics Laboratory, NASA's Goddard Space Flight Center, Code 667, Greenbelt MD 20771 USA*

[3]*Department of Terrestrial Magnetism, Carnegie Institution of Washington, 5241 Broad Branch Road NW, Washington, DC 20015 USA*

[4]*Center for Radiophysics and Space Research, Cornell University, 326 Space Sciences Bldg., Ithaca, NY 14853-6801 USA*

Abstract. Recent Spitzer infrared (IR) observations of two transiting hot Jupiters during their secondary eclipses have provided the first direct detection of planets orbiting other stars (Charbonneau et al. 2005; Deming et al. 2005). We here elaborate on some aspects of our detection of HD 209458b at 24 μm, and we compare to the detection of TrES-1 by Charbonneau et al. Spitzer will eventually determine the IR spectral energy distribution of these and similar hot Jupiters, opening the new field of comparative exoplanetology. For now, we have only three Spitzer data points, augmented by upper limits from the ground. We here interpret the available measurements from a purely observational perspective, and we point out that a blackbody spectrum having $T \sim 1100$K can account for all current IR measurements, within the errors. This will surely not remain true for long, since ongoing Spitzer observations will be very sensitive to the IR characteristics of hot Jupiters.

1. Direct detection of extrasolar planets

There are now over 160 extrasolar planets known from Doppler surveys, and about 15% of these are hot Jupiters. Strong stellar irradiation heats these planets to $T > 1000$K (Seager and Sasselov 1998), so they should emit most of their radiation in the IR. A number of pioneering attempts were made to detect hot Jupiters from the ground in the combined IR light of star+planet (Wiedemann et al. 2001, Lucas and Roche 2002, Richardson et al. 2003a,b). But success was only recently achieved, and it required using the Spitzer Space Telescope (Charbonneau et al. 2005; Deming et al. 2005).

The Spitzer observations of two hot Jupiters are the first direct detections of extrasolar planets. To be clear about terminology, by direct detection we mean that photons emitted by the planet are detected, and are separated from stellar photons by some method. One method to separate the stellar and planetary photons would be to spatially resolve the planet and the star, e.g., by imaging. Imaging of extrasolar planets is being widely pursued, but it requires a very high order of technology. The technique which is successful for Spitzer is to observe the *secondary eclipse* of transiting hot Jupiters. We measure the star+planet when the planet is out of eclipse, and the star alone when the planet is eclipsed, and the difference tells us how many photons are due to the planet.

Note that the secondary eclipse technique does not specify *which* of the detected photons are due to the planet, and which are from the star, only *how many* photons are from the planet. But for scientific purposes, 'how many' is the primary quantity of interest! So secondary eclipses are a very sensitive and useful method for direct detection and characterization of transiting extrasolar planets. There are *nine* ongoing Spitzer programs to detect and characterize close-in extrasolar planets in combined IR light, and we are now truly in the era of comparative exoplanetology.

In Section 2, we describe our detection of the secondary eclipse of HD 209458b, elaborating on some points not mentioned in our detection paper. Section 3 interprets our results in combination with the TrES-1 measurements by Charbonneau et al. (2005), and factors in the ground-based upper limits. We point out the importance of measuring these planets in the 2- to 5-μm wavelength region, where there is currently a considerable question about their level of IR emission.

2. The secondary eclipse of HD 209458b

Figure 1 shows the secondary eclipse of HD 209458b at 24 μm wavelength, observed using the Multiband Imaging Photometer for Spitzer

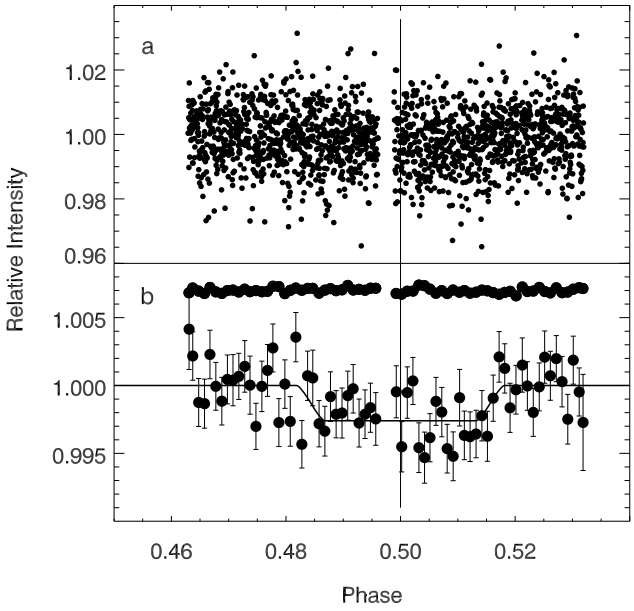

Figure 1. *Photometric detection of the secondary eclipse of HD 209458b using Spitzer/MIPS. The upper panel shows all 1696 individual photometric points, which are binned in the lower panel to show the eclipse. The fitted eclipse curve is overplotted. The points above the eclipse are a control sequence, showing the stability of the technique. Note that the eclipse is accurately centered at phase 0.5, as marked by the vertical line.*

(MIPS, Rieke et al. 2004). The scatter in the individual points (upper panel) is about 0.008 magnitudes, poorer than is possible from the ground in the visible. However, the MIPS precision is limited by statistical fluctuations in the thermal emission from dust in our own solar system, the IR zodiacal light. The Spitzer data analysis pipeline provides an 'error image' which quantifies these statistical fluctuations. We extract the brightness of the star using an optimal weighting technique (Horne 1986), and we propagate the error image thru the same procedure to derive the formal errors in the photometry. We find the scatter in our photometry to be in close agreement with the formal errors. We are background-limited by the thermal zodiacal emission.

In addition to noise from the zodiacal background, there are some instrument quirks in MIPS. For example, there is a 'first frame' effect, where the signal from the MIPS detector is different if it has just been

reset. Fortunately, we were able to use a simple trick to remove the instrument quirks. Our trick is to ratio the intensity of the star to the total intensity of the zodiacal background in the image. Since the background is a large signal, its relative precision is much better than the star's precision, and the ratio does not add significant additional noise. Moreover, because of Spitzer's modest (0.85-meter) aperture, diffraction spreads the stellar image over multiple pixels, like the background. Also, the per-pixel intensity of the star is only modestly greater than the background. To MIPS, the star looks like a small patch of bright background, so the instrument treats the background and stellar photons exactly the same - it cannot 'tell the difference'. After normalizing the stellar intensity to the background, we find the instrument quirks are gone, and the noise is accurately characterized as Gaussian white noise, which averages down as the square-root of the number of observations - just as the text books predict.

The lower panel of Figure 1 averages our secondary eclipse photometry into bins of 0.001 in phase, and adds error bars to the binned values. Now the secondary eclipse is quite evident, and is seen to be centered at phase 0.5. We fit an eclipse curve to the data, and find a best-fit depth of $0.26 \pm 0.046\%$, a 5.6σ detection. The planet's brightness temperature is 1130 ± 150K. Simultaneously with our MIPS detection of HD 209458b, Charbonneau et al. (2005) detected TrES-1 at 8- and 4.5-μm using Spitzer's InfraRed Array Camera (IRAC). The TrES-1 measurements imply a very similar temperature (1060K), and their 8 μm measurement has over 6σ statistical significance. Since these three data points are (so far) our only direct measurements of hot Jupiters, they have elicited considerable interest. Four modeling papers have interpreted the measurements (Barman et al. 2005, Burrows et al. 2005, Fortney et al. 2005, Seager et al. 2005), but in Sec. 3 we will give a more simple-minded interpretation, highlighting what we call the 'short IR wavelength question'.

The Spitzer detections have been described as surprising, in the sense of being unexpected. Certainly this application for Spitzer was unanticipated in the early years when the observatory was being developed. But recently, the planet-to-star contrast ratio was robustly predicted to be a significant fraction of one percent at long IR wavelengths (Charbonneau 2003, Burrows et al. 2004). Prior to launch, we reasoned that if we couldn't detect a fraction of one percent using a cryogenic telescope in space, then we should surely give up! Fortunately, the first public data from MIPS showed us that Spitzer's sensitivity and stability were up to the task. So we knew in advance that we would detect HD 209458b with MIPS, providing that the planet was at least as hot as 700K - which seemed unavoidable.

Curiously, the Spitzer detections did not start with the best cases. Since the flux from both the planet and star decrease with wavelength (decline of the Planck function), 24 μm is not the best wavelength for secondary eclipse detection. The IRAC 8 μm channel is more suitable, being source photon-limited, not background-limited. But for historical reasons, IRAC was first used by Charbonneau et al. for TrES-1, not for HD 209458. So the brighter and closer system was not observed at the best wavelength. The new observing programs now underway will soon fill this gap, and we will see secondary eclipses of hot Jupiters even more clearly. The new very hot Jupiter recently announced by Bouchy et al. (2005) will be an especially important target for Spitzer.

3. The short IR wavelength question

3.1 New 3.8 μm photometry

In order to discuss what we regard as the major unresolved observational question concerning hot Jupiters, we need to include the ground-based data. A flux peak is predicted to occur in hot Jupiter spectra at 3.8 μm (Sudarsky et al. 2003). Ground-based observations can be very useful at this important wavelength, because we can use a filter centered exactly on the predicted peak (the IRAC bandpasses are offset). Unfortunately, the high thermal background from the ground has made broadband photometry impossible near 4 μm - most instrument detector arrays saturate in quite short integration times.

In September 2003 we obtained 3.8 μm photometry of HD 209458 during two secondary eclipses, using NSFCAM (Shure et al. 1994) on the NASA Infrared Telescope Facility (IRTF). We were able to avoid detector saturation by using a narrow optical bandwidth, a 1.5% circular-variable-filter (CVF). Figure 2 shows the atmospheric transmittance, and the profile of the conventional L′ filter, and our CVF at 3.8 μm. To monitor changes in atmospheric absorption, we observed a comparison star of similar brightness to HD 209458. We have completed the analysis of one of the two eclipses. The eclipse amplitude in that case, from 329 individual 10-second exposures, was -0.0007 ± 0.0014, i.e. the system nominally becomes brighter when the planet is hidden, consistent with seeing no eclipse. Not surprisingly, the errors are larger in the ground-based observations than with Spitzer, but nevertheless the results are sufficiently precise to be somewhat puzzling, as we explain below.

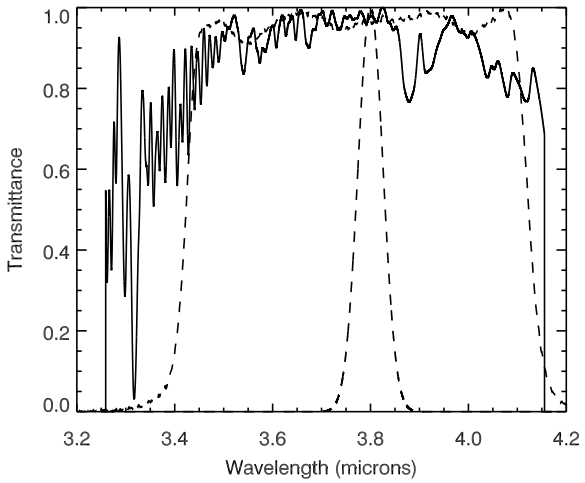

Figure 2. *Window in the terrestrial atmosphere for photometry of hot Jupiters at 3.8 μm. The solid line shows the telluric transmittance at moderate spectral resolution. The dashed curves are the transmittance of the conventional L′ filter (broad), and our CVF (narrow).*

3.2 An observational perspective

The two extrasolar planets currently observed by Spitzer - HD 209458b and TrES-1 - are different worlds, and they surely have their own unique characteristics. But, our ignorance of hot Jupiter spectra is arguably much greater than the real differences between them. So here we compare observations of both planets to a single model. To quantify the similarity between the two planets, we assume thermal equilibrium and the same Bond albedos and efficiency of heat redistribution. In the long wavelength (Rayleigh-Jeans) limit, it is easy to show that the planet-to-star contrast c_λ depends on the stellar and orbital parameters as:

$$c_\lambda \sim R_p^2 R_*^{-\frac{3}{2}} a^{-\frac{1}{2}} \tag{1}$$

where R_p and R_* are the planetary and stellar radius, respectively, a is the orbit semi-major axis, and we suppress the constant containing the Bond albedo. Note that the temperature of the star does not appear since it cancels when computing the contrast. Using the parameters for HD 209458 (Brown et al. 2001; Wittenmyer 2005) and TrES-1 (Alonso et al. 2004), we find that the contrasts for these two systems at a given wavelength would differ by only 8% under our simple assumptions. So comparing them to a single model is reasonable.

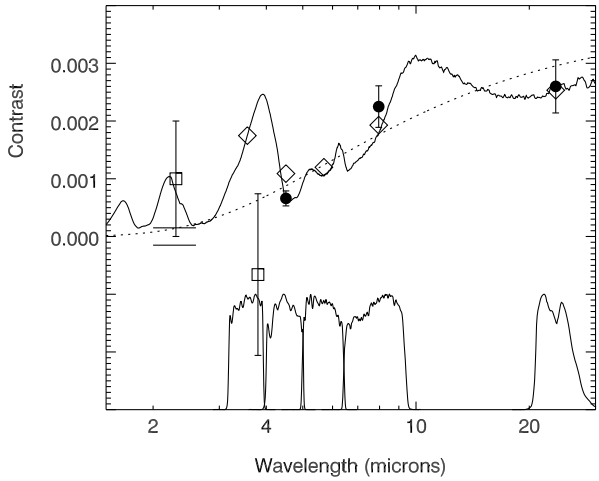

Figure 3. *Spitzer and ground-based observations of TrES-1 and HD 209458b in contrast units, compared to a single model (solid line) and 1100K blackbody (dotted line). The Spitzer IRAC and MIPS bandpass functions are plotted below. Filled symbols are the Spitzer points, and the open diamonds show the expectation value of the contrast averaged over the Spitzer bands. The open squares show the ground-based photometry of Snellen (2005) at 2.3 μm, and from this paper at 3.8 μm. The two horizontal lines at 2.2 μm represent the limit from Richardson et al. (2003b). Note log scale for wavelength.*

Figure 3 shows contrast versus wavelength for HD 209458b and TrES-1, and compares the observations to a model from Sudarsky et al. (2003), as did Charbonneau et al. (2005, their Figure 3). The dashed line is the contrast from a blackbody having $T = 1100$K. The Spitzer observations cannot in themselves discriminate between the model curve and a simple blackbody. Considering the errors, all three Spitzer observations could be consistent with either the Sudarsky et al. model or the blackbody.

Now we consider the ground-based data. The error bar on our CVF photometry at 3.8 μm misses the Sudarsky et al. peak at this wavelength, but it overlaps the blackbody. The Snellen (2005) photometry at 2.3 μm agrees with the model, but the error bar also includes the blackbody curve. The most stringent ground-based point is the Richardson et al. (2003b) upper limit at 2.2 μm. This is a limit, derived from differential spectroscopy, on the shape of the spectrum, and it is given by the two horizontal lines. Unlike the other error limits on

the figure, this is a 3σ, not 1σ limit. These lines are relative limits, i.e. only the intensity interval between them is significant (see Seager et al. 2005). To conform to this limit, the contrast spectrum has to fit within the lines. The Sudarsky et al. model doesn't fit, but the blackbody does. This is the essence of the short-IR wavelength question - we don't see the peaks predicted in the spectrum where planet flux should escape between absorption bands, and we wonder how strong these peaks really are. Now, we do not seriously suggest that the planet is actually a blackbody. But to date, we do not have a definitive measurement of departures from a blackbody spectrum in the IR. The IRAC band at 3.5 μm should provide this, as evident from Figure 3. Observations of TrES-1 at 3.5 μm were made by Spitzer in September 2005, and are now being analyzed by Dave Charbonneau. We eagerly await the results.

References

Alonso, R., *et al.*, 2004, ApJ 613, L153

Barman, T. S., Hauschildt P. H., & Allard, F. 2005, ApJ 632, 1132

Bouchy, F., *et al.*, 2005, A&A, 444, L15

Brown, T. M., Charbonneau, D., *et al.*, 2001, ApJ 552, 699

Burrows, A., Hubeny, I., & Sudarsky, D. 2005, ApJ 625, L135

Burrows, A., Sudarsky, D., & Hubeny, I. 2004, in *The Search for Other Worlds*, AIP Conf. Proceedings, 713, 143

Charbonneau, D. 2003, in *Scientific Frontiers in Research on Extrasolar Planets*, ASP Conf. Series, 294, 449

Charbonneau, D., *et al.*, 2005, ApJ 626, 523

Deming, D., Seager, S., *et al.*, 2005, Nature 434, 740

Fortney, J. J., Marley, M. S., Lodders, K., *et al.*, 2005, ApJ 627, L69

Horne, K. 1986, PASP 98, 609

Lucas, P. W. & Roche, P. E. 2002, MNRAS 336, 637

Richardson, L. J., *et al.*, 2003a, ApJ, 154, 583

Richardsom, L. J., Deming, D., & Seager, S. 2003b, ApJ 597, 581

Rieke, G. H., *et al.*, 2004, ApJ(Suppl) 154, 25

Seager, S. & Sasselov, D. D. 1998, 502, L157

Seager, S., Richardson, L. J., *et al.*, 2005, ApJ 632, 1122

Shure, M. A., Toomey, D. W., *et al.*, 1994, SPIE 2198, 614

Snellen, I. A. G. 2005, MNRAS 363, 211

Sudarsky, D., Burrows, A., & Hubeny, I. 2003, ApJ 588, 1121

Wiedemann, G., Deming, D., & Bjoraker, G. 2001, ApJ 546, 1068

Wittenmyer, R. A., *et al.*, 2005, ApJ 632, 1157

Tenth anniversary of 51 Peg-b : Status of and prospects for hot Jupiter studies
Proceedings of Haute Provence Observatory Colloquium (22-25 August 2005)
Edited by L. Arnold, F. Bouchy, and C. Moutou

Evaporation of hot Jupiters: observations and models

R. Ferlet, J.-M. Désert, G. Hébrard, A. Lecavelier des Etangs, and A. Vidal–Madjar

Institut d'astrophysique de Paris, UMR7095 CNRS, Université Pierre & Marie Curie, 98bis Bd. Arago, 75014 Paris, France [ferlet@iap.fr]

Abstract. We report the detection of the exosphere of the extrasolar planet HD 209458 b through transmission spectroscopy with the HST. The extra-absorptions measured during the transit in hydrogen, oxygen and carbon imply that the atmosphere is evaporating through an hydrodynamic "blow–off" mechanism. The escape rate and the lifetime of hot Jupiters are estimated from a particular modeling. It is suggested that some of the less massive known exoplanets could be the dense cores remnants of such an evaporation process.

1. Introduction

Ten years after the discovery of the first Jupiter-sized object orbiting a star other than the Sun (51 Peg b, Mayor & Queloz 1995), nearly 170 extrasolar planets have now been detected, mainly thanks to the radial velocity method. Amongst them, about 15% (including 51 Peg b) have very short-period orbits, less than 0.1% of Jupiter's. With corresponding semi-major axis a as low as $\sim$ 10 stellar radii R_*, these hot Jupiters have a probability $P \approx R_*/a$ of the order of 1/10 to transit across the disk of a Sun-like star. The first transiting extrasolar planet, HD 209458 b, was found in 1999 (Charbonneau et al. 2000; Henry et al. 2000), with the stellar flux decreasing by 1.64% during the 2.4 hours transit. Such a case is very favourable for applying the transmission spectroscopy technique in order to detect absorption features in the spectrum of the parent star due to the planet's atmosphere. Thus, Charbonneau et al. (2002) identified the presence of sodium in the dense lower atmosphere of HD 209458 b, and measured a photometric dimming during transit in the sodium bandpass deeper by (2.32 ± 0.57)

10^{-4} relative to adjacent bands. Using the same technique, we have further explored the upper atmosphere of HD 209458 b.

2. First detection of the exosphere of an extrasolar planet

Hydrogen escape is a well known phenomenon for the telluric planets of the solar system. In particular, the Earth is loosing about 200 tons of hydrogen atoms per year through the Jeans mechanism: at the exobase - level above which collisions become negligible - H atoms are ballistic and those with a sufficient thermal velocity in the tail of the Maxwellian velocity distribution can escape. For the giants planets, on the contrary, their temperature is too low and their gravity too strong for allowing any escape.

As soon as 51 Peg b was announced, Burrows & Lunine (1995) questioned the possibility of planetary evaporation, and concluded that Jeans escape should be negligible. However, they added that another type of escape could be at work and estimated an evaporation rate of 10^{10} g.s^{-1}. Further theoretical studies (see e.g. Guillot et al. 1996; Seager & Sasselov 2000; Brown 2001) evaluate the planetary effective temperature and agree on $T_{eff} \sim 1400$ K, which is not enough to allow Jeans escape.

In spite of this pessimistic context, it seemed to us that hydrogen, the lightest and most abundant element, could be the best tracer to detect an upper atmosphere. In its ground level, the strongest H I line is Lyman α at 1216 Å, the only one available with the Hubble Space Telescope. HD 209458 being a solar type star, it was quite easy to predict its Lyman α profile and the putative supplementary absorption due to H atoms in the planetary exosphere. The proposal has been accepted. The observed spectra are shown in Figure 1.

The signature of atmospheric neutral hydrogen has been detected in absorption during the planetary transit. From a very sophisticated data analysis, it turns out that 15% of the stellar light is occulted during the transit, to be compared to the 1.6% observed in the visible continuum (1.35 $R_{Jupiter}$ = 96 500 km). As a matter of fact, this extra-absorption corresponds to a total of 135 lacking photons during three different transits, which translates into a 4.5 σ detection of the upper atmosphere of HD 209458 b.

If the whole Roche lobe of the planet was filled with hydrogen, then the occultation should have been 10% of the stellar disk (R_{Roche} = 3.6 $R_{Jupiter}$). Thus, the observed 15% absorption (4.3 $R_{Jupiter}$ = 300 000 km) implies that the atmosphere in hydrogen extends beyond the Roche lobe; atoms are not any more gravitationally bound to the planet and therefore are escaping. Moreover, absorption is seen down to

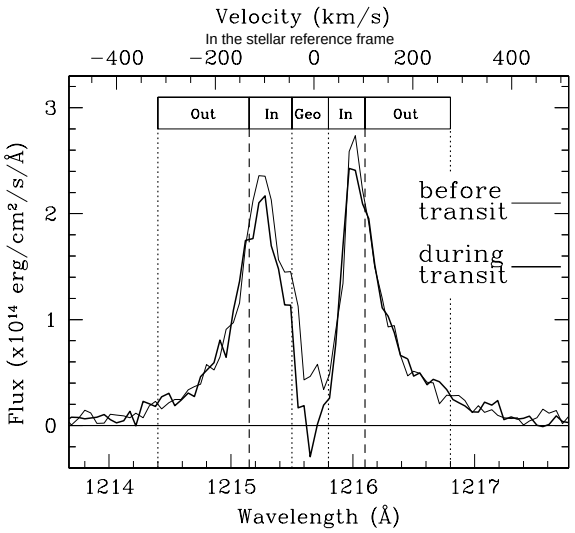

Figure 1. *Lyman α profile of HD 209458 as observed with the medium resolution STIS spectrograph G140M on-board the Hubble Space Telescope (Cycle 10). Thin line is the mean spectrum before the transit and thick line is during the transit. Three different bandpasses are identified: "Geo" is the domain where geocoronal emissions occur (it is excluded from the analysis, but it is worthwhile to note that its inclusion does not alter the final result); "In" and "Out" are the inner and outer domains of the stellar Lyman α line. Significant variations are detected only in the "In" domain, between -130 and +100 km.s^{-1} (stellar reference frame). An absorption of 15 ± 4% is measured (Vidal–Madjar et al. 2003).*

-130 km.s^{-1}. The escape velocity of the planet being 54 km.s^{-1}, atoms have velocities large enough to escape. From these two independent assessments, one unavoidably concludes that the planet is evaporating.

In order to evaluate the evaporation rate, we have conducted a numerical simulation by taking into account both the planetary and stellar gravities, and the stellar Lyman α radiation pressure known to be 0.7 times the stellar gravity. The two free parameters are the lifetime and the volume density at the exobase of neutral hydrogen. With an H$\tilde{\text{I}}$ mean free path of the order of the Roche lobe, the volume density can be estimated to be about 10^6 atoms.cm^{-3}. The H I lifetime is limited to $\approx$ 6 hours due to ionisation by the stellar extreme UV flux, after

scaling from the known lifetime in the solar system. The escaping atoms expand in an asymmetric comet-like tail and progressively disappear when moving away from the planet. To account for the observed 15% absorption depth, the particle simulation implies a minimum escape flux of 10^{10} g.s^{-1}. Note however that owing to saturation effects in absorption lines, a flux larger by two orders of magnitude would not significantly affect the observed profile.

3. New observations

Beyond hydrogen, the lightest and most abundant element is helium. However, He has no observable resonant transitions, and it is hopeless to search for excited transitions in an exosphere; mostly populated by collisions, these excited levels will occur only in the much denser lower atmosphere. The H_2 molecule could be observable through ground transitions, but in the far UV where solar type stars are almost dark. Deuterium too, but it would be hidden in the wide H I absorption. We therefore looked for heavier elements still abundant: ionised carbon (C I being easily ionised in the upper atmosphere), neutral oxygen (ionisation potential similar to that of hydrogen and thus protected by large amounts of H I above it), and nitrogen (but difficult because of its lines about 1000 times weaker than Lyman α). The new observed spectra are shown in Figure 2.

The hydrogen signature of the exosphere of HD 209458 b is confirmed. The extra absorption during the transit is $\approx 5\%$, totally compatible with the previous results when taking into account the much lower spectral resolution of these new observations. Moreover, oxygen and carbon are also present in the upper atmosphere, up to the Roche lobe ($\sim$ 10% absorption). Their mere detection implies that the planet is effectively evaporating, but not under a Jeans mechanism. Only an extremely efficient process can transport such heavy atoms at high altitude, an hydrodynamic escape or "blow–off" (Chamberlain & Hunten 1987). These atoms are carried away within the hydrogen flow with a velocity $10 km.s^{-1}$, close to the sound velocity. As a matter of fact, a similar type of violent escape should have occurred on the primitive Earth, explaining thus the quasi-absence of rare gases in our atmosphere (Chassefière 1996a, 1996b).

We have also identified absorption signatures from the metastable transitions O I*, O I** and C II*. These are excited only through collisions, which proves that at the location where these atoms are observed the volume density is at least the one at the exobase (by definition, the exobase is the level above which collisions become negligible). Therefore, at the level of the Roche lobe the volume density should be $\sim 10^6$

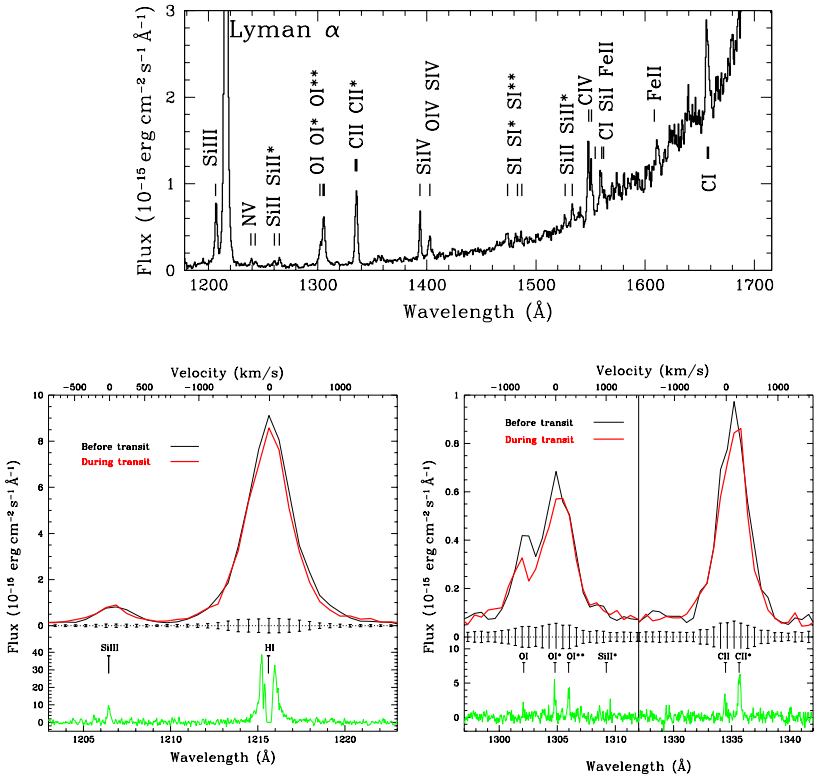

Figure 2. *Top : Overall spectrum of HD 209458 as observed with the low resolution STIS spectrograph G140L on-board the Hubble Space Telescope (Cycle 12). Bottom : Zoom of the H I, Si III, O I and C II lines. Thin lines are the spectra before the transit and thick lines are during the transit. Significant variations are detected only in H I, O I and C II. For these last two, absorptions include the excited transitions O I*, O I** and C II*. Below : Echelle spectrum at very high resolution. (Vidal–Madjar et al. 2004).*

atoms.cm^{-3}. A similar value is independently derived from the evaluation of the optical depth for the observed lines. The exobase is thus very likely in the vicinity of the Roche lobe. The escape rate is equal to the flux of hydrogen atoms flowing through the surface of the Roche lobe. We easily derive a rate 1.3 $10^{10} g.s^{-1}$, in excellent agreement with the above independent estimation!

4. Modeling the atmospheric escape

Lecavelier des Etangs et al. (2004) have built models of the atmospheric evaporation by assuming two important conditions: first, the temperature of the upper atmosphere (T_{up}) is not equal to the effective temperature and second, tidal forces induced by the close-by parent star are significant. Note for instance that the temperature of the upper atmosphere of Jupiter is $\approx$ 1000 K, well above its T_{eff} and still unexplained. They compute the escape rate as a function of temperature, and from an escape rate $10^{10} g.s^{-1}$, they derive $T_{up} \simeq 8000$ K.

It is possible to roughly estimate the increase of the temperature toward the upper atmosphere by balancing the heating and cooling processes possibly at work. Heating is due to the stellar UV (Lyman α) and EUV radiations. Cooling occurs through thermal conduction, collisional excitation of H I levels, collisional ionisation and of course escape. Lecavelier des Etangs et al. (2004) have computed the exospheric temperature as a function of the orbital distance of the planet and identified two different regimes. Away from the star down to about 0.1 AU, the EUV heating gradually sets up the Jeans escape domain. At shorter distances, temperature is exceeding $\sim$ 10 000 K and the "blow–off" regime dominates, which then leads to a sharp escape cooling. As we have directly observed a "blow–off", T_{up} should be above $\sim$ 10 000 K, implying then an escape rate larger than $\sim 10^{10}$ g.s^{-1}.

The obvious question is then the lifetime of hot Jupiters with respect to the evaporation mechanism. Lecavelier des Etangs et al. (2004) computed iso-lifetime curves in a plot planet mass versus orbital distance (Figure 3). Massive Jupiters can survive very nearby their parent star. HD 209458 b lifetime is of the order of the lifetime of its star and will loose through evaporation at most few % of its mass. Less massive planets will not survive too close to their star. The black area in Figure 3 is the location where planets are modified during the lifetime of their star. The dark area at the very bottom of Figure 3 indicates the location of the plausible remnants when the evaporation process is completed.

5. Conclusions

The observational discovery of the evaporation mechanism at work in the atmosphere of an extrasolar planet – made, as a matter of fact, while some theories were predicting that mechanism to be very unlikely – opens new ways of thinking. New observations were planned, but unfortunately, the STIS instrument on-board the HST is presently out of service. We are waiting for data from the ACS instrument to test

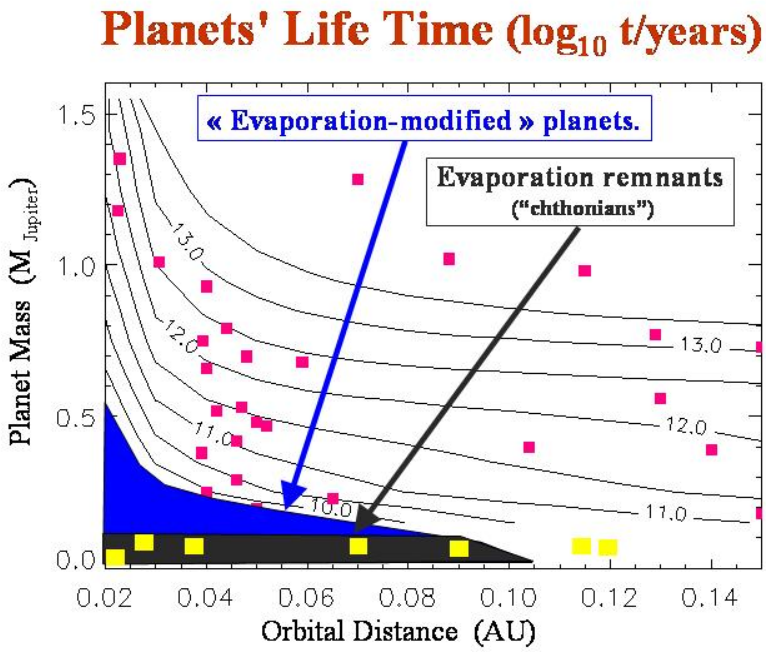

Figure 3. *Iso-lifetime curves as a function of the exoplanet initial mass (in units of $M_{Jupiter}$) and orbital distance (in UA)(e.g. the curve indicated 12.0 means a lifetime of 10^{12} years). Within the black area, the time needed to totally evaporate the hydrogen atmosphere of a planet is shorter than 10^9 years. Computation takes into account the time evolution of masses, radii and effective temperatures as estimated by Guillot (2005), as well as the time evolution of the FUV/EUV stellar flux. Small squares represent some of the known extrasolar planets. Big squares are the known exoplanets with the smallest masses (less than 21 Earth masses). They are located in a dark area in which only dense cores of initial hot Jupiters can survive (Lecavelier des Etangs et al. 2004).*

the feasibility of exospheric studies with it. While giant planets are formed beyond their ice limit, they rapidly migrate inwards, until the evaporation process is ignited and eventually dominates the evolution of the planet. Perhaps it is a way to explain why very hot Jupiters seem to pile up at roughly the same distance from their parent star. One is then led to predict the existence of a new type of planets we suggest to

call "chtonians" planets (by reference to the Greek god "Kthon", deity of internal worlds), the remnants dense cores possibly already detected (the bottom left big squares in Figure 3).

References

Brown, T. 2001, ApJ, 553, 1006.

Burrows, A., & Lunine, J. 1995, Nature, 378, 333.

Chamberlain, J., & Hunten, D. 1987, in *Theory of Planetary Atmospheres : An Introduction to Their Physics and Chemistry*, Int. Geophys. Ser. 36, 2nd ed. 2; Orlando: Academic.

Charbonneau, D., Brown, T., Latham, D., Mayor, M., & Mazeh, T. 2000, ApJ, 529, L45.

Charbonneau, D., Brown, T., Noyes, R., & Gilliland, R. 2002, ApJ, 568, 377.

Chassefière, E. 1996a, Icarus, 124, 537.

Chassefière, E. 1996b, JGR, 101, 26039.

Guillot, T., Burrows, A., Hubbard, W., Lunine, J. & Saumon, D. 1996, ApJ, 459, L35.

Guillot, T. 2005, Annual Review of Earth and Planetary Sciences, 33, 493.

Henry, G., Marcy, G., Butler, P., & Vogt, S. 2000, ApJ, 529, L41.

Lecavelier des Etangs, A., Vidal–Madjar, A., McConnell, J. & Hébrard, G. 2004, A&A, 418, L1.

Mayor, M., & Queloz, D. 1995, Nature, 378, 355.

Seager, S., & Sasselov, D. 2000, ApJ, 537, 916.

Vidal–Madjar, A., Lecavelier des Etangs, A., Désert, J.-M., Ballester, G., Ferlet, R., Hébrard, G., & Mayor, M. 2003, Nature, 422, 143.

Vidal–Madjar, A., Désert, J.-M., Lecavelier des Etangs, Hébrard, G., Ballester, G., Ehrenreich, D., Ferlet, R., McConnell, J., Mayor, M. & Parkinson, C. 2004, ApJ, 604, L69.

Tenth anniversary of 51 Peg-b : Status of and prospects for hot Jupiter studies
Proceedings of Haute Provence Observatory Colloquium (22-25 August 2005)
Edited by L. Arnold, F. Bouchy, and C. Moutou

Comparative planetary atmospheres: models of HD 209458b, TrES-1, and HD 149026b

J.J. Fortney[1], M.S. Marley[1], D. Saumon[2], K. Lodders[3], and R.S. Freedman[1,4]

[1]*Space Science and Astrobiology Division, NASA Ames Research Center, MS 245-3, Moffett Field, CA 94035 [jfortney@arc.nasa.gov]*

[2]*Los Alamos National Laboratory, MS F699, Los Alamos, NM 87545*

[3]*Planetary Chemistry Laboratory, Department of Earth and Planetary Sciences, Washington University, St. Louis, MO 63130*

[4]*SETI Institute, 515 N. Whisman Road, Mountain View, CA 94043*

Abstract. We present new self-consistent atmosphere models for transiting planets HD 209458b, TrES-1, and HD 149026b, and compare the planets' pressure-temperature profiles and infrared spectra. Their atmospheres likely span a range of $T_{\rm eff}$ from $\sim$1100 to 1750 K (and may reach up to 2100 K). HD 209458b and TrES-1 were recently observed with the *Spitzer Space Telescope*. We compare our spectra to the *Spitzer* observations and discuss what deviations from standard solar composition atmospheres are needed. Hot stratospheres may be present in these atmospheres, especially for the hottest planet, HD 149026b.

1. Introduction

The detection of photons emitted by an extrasolar planet is a landmark feat in the history of astronomy. Ten years after the initial discovery of the first extrasolar giant planet (EGP) 51 Peg b (Mayor & Queloz, 1995), Charbonneau et al. (2005) report the detection of infrared flux from TrES-1 and Deming et al. (2005) report a similar detection for HD 209458b. Both observations were made with the *Spitzer Space Telescope* as each planet passed behind its parent star. While a number of papers

have aimed at predicting the optical and infrared spectra of Pegasi planets (hot Jupiters) (Seager and Sasselov 1998, Marley et al 1999, Barman et al 2001, Sudarsky et al 2003, Iro et al 2005), these results are the first infrared detections (rather than upper limits) that can be compared with models.

2. Methods

To obtain our atmospheric pressure-temperature (P–T) profiles and spectra for the planets we employ a 1D model atmosphere code that has been used for a variety of planetary and substellar objects (Mc Kay et al 1989, Marley et al 1996, Burrows et al 1997, Marley and Mc Kay 1999, Marley et al 2002) and we are now using it to model the atmospheres of Pegasi planets. Details can be found in Fortney et al (2005a, 2005b). The code explicitly includes both incident radiation from the parent star and thermal radiation from the planet's atmosphere. We use the elemental abundance data of Lodders (2003) and compute chemical equilibrium compositions following Fegley and Lodders (1994) and Lodders (2002). We predict all cloud properties using the model of Ackerman and Marley (2001) with a sedimentation efficiency parameter $f_{sed} = 3$. All the relevant planetary parameters for TrES-1 are taken from Sozetti et al (2004), for HD 209458b from Brown et al (2001), and for HD 149026b from Sato et al (2005). For the stellar fluxes we use Kurucz model atmospheres (Kurucz, 1993).

3. Model Profiles and Spectral Signatures

We first show P–T profiles for all three planets, then spectra, then planet-to-star flux density ratios for nominal planet characteristics. Fig. 1 shows P–T profiles for the three planets, assuming solar metallicity. These profiles all assume an intrinsic temperature ($T_{\rm int}$, the $T_{\rm eff}$ of the planet if it were in isolation) of 100 K. These profiles all assume efficient redistribution of absorbed stellar flux around the entire planet. In practice in a 1D atmosphere code, this means the incident stellar flux is diluted by a factor of 1/4 (see Fortney et al 2005b). The radiative zone extends deepest in HD 149026b because it receives the greatest incident stellar flux. HD 149026b receives 5 times more stellar flux than TrES-1, so we should expect appreciable differences in the model atmospheres. The profile for TrES-1 is quite close to the curve where CH_4 and CO have the same abundance. For TrES-1, most carbon is in the form of CO but an appreciable mixing ratio of CH_4 is expected. For all of these profiles, the normal optical depth reaches unity (i.e. the

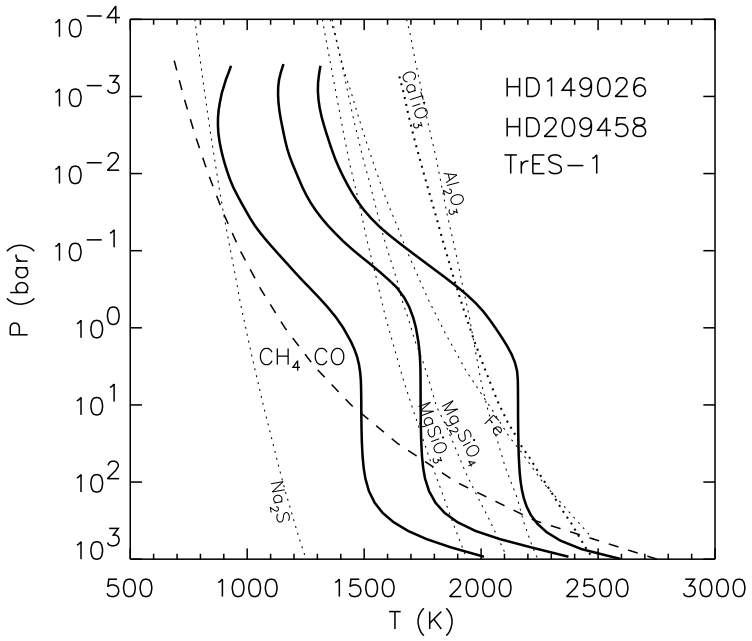

Figure 1. *Pressure-temperature profiles, from left to right, for TrES-1, HD 209458b, HD 149026b. Relevant condensation curves are shown. Solar metallicity is assumed.*

"photosphere") at ~10-300 mbar for all wavelengths between 3 and 30 μm, which is fairly high in the planets' atmospheres.

The infrared spectra of these Pegasi planets are dominated by H_2O, CO, and for TrES-1, also CH_4. As shown in Fig. 2 the emergent spectra of HD 149026b and HD 209458b are fairly similar. However, TrES-1 shows absorption due to CH_4 at 3.3 μm and from 7-9 μm.

The planet-to-star flux density ratios fold in the flux of the star, the flux of the planet, and the surface area ratios. For these standard solar-metallicity atmospheres, Fig. 3 shows that our model is an excellent fit to the Deming et al (2005) HD 209458b observation at 24 μm. For TrES-1, our model fits the Charbonneau et al (2005) observations reasonably well. At 4.5 μm, the model is at the 1σ error bar, but is 2-3σ too low at 8.0 μm. The infrared spectral slope of TrES-1 is redder than we predict—and somewhat redder than a blackbody (see Charbonneau et al 2005). [2] We find that models with a higher metallicity ([M/H]=0.5) or

[2]Deming (this volume) suggests additional evidence for blackbody-like spectra for Pegasi planets can be found from the ground-based secondary eclipse non-detections

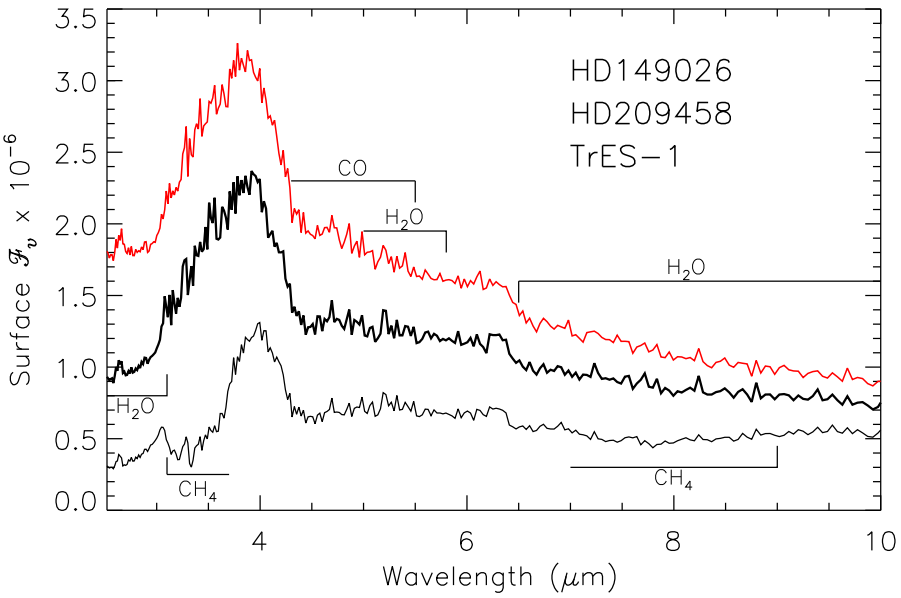

Figure 2. *Emergent spectra for the three planetary P–T profiles shown in Fig. 1. From top to bottom the spectra are HD 149026b, HD 209458b, TrES-1. Relevant molecular absorption features are labeled.*

models with a hot stratosphere at pressures less than ∼50 mbar improve the fit to observations, as the atmosphere becomes brighter in the 8.0 μm band, while the flux from the 4.5 μm band remains essentially constant. Observations at 5.8 μm should give us more information on the spectral slope and observations at 3.6 μm should show if the predicted flux peak at 4 μm does indeed exist (Fortney et al 2005). We note that models of the infrared spectra of M, L, and T dwarfs (which have $T_{\rm eff}$s similar to Pegasi planets) are an excellent fit to *Spitzer* IRS spectra from ∼5-15 μm (Roelling et al 2004).

A closer look at atmosphere models of HD 149026b is warranted, given its peculiarly large bulk mass fraction of heavy elements (Sato et al 2005, Fortney et al 2005b). Model atmospheres with higher metallicity are warmer, as a greater percentage of incoming flux is absorbed. (This absorption is greater than 90% for models of Pegasi planets.) Fig. 4

---

of HD 209458b by Richardson et al (2003) at 2.2 μm and by Deming at L-band. A blackbody-like spectrum could be due to an isothermal atmosphere or the opacity of an optically thick cloud high in the planet's atmosphere.

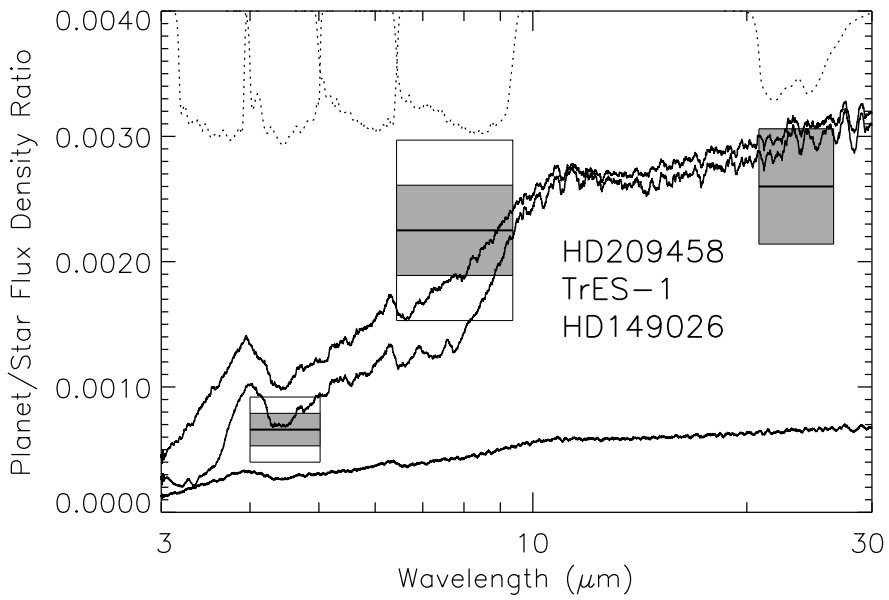

Figure 3. *Planet-to-star flux density ratios for, from top to bottom, HD 209458b, TrES-1, and HD 149026b. Spitzer data are shown—shaded areas are 1 σ error bars, and open boxes are 2 σ error bars. The 4.5 and 8.0 μm data are for TrES-1and the 24 μm datum is for HD 209458b. Spitzer IRAC and MIPS bands are shown as dotted lines at the top.*

shows profiles with metallicities of [M/H]=0.0 and [M/H]=0.5 which cross the condensation curve of $CaTiO_3$ (shown in the figure for solar metallicity), implying that most TiO will be tied up in this condensate at high pressure. Here, as a simplified way to explore the consequences of this issue, we remove TiO at all pressures less than 10 bars. (For a complete exploration of titanium chemistry in substellar atmospheres see Lodders (2002).) For an even higher metallicity atmosphere, or for a hot day side (and a corresponding cold night side) these profiles *may* be warmer than the condensation curve of $CaTiO_3$. (This depends on the exact $T_{\rm int}$ of the planet.) However, at higher metallicity the $CaTiO_3$ condensation curve is shifted parallel from the solar curve to higher temperature. To the right of this curve, gaseous TiO will be free in the atmosphere. Since TiO is a strong absorber in the visible, a hot stratosphere is formed as nearly all incident visible flux is absorbed at low pressure. These profiles with hot stratospheres have dramatically different spectra that our previous models, as shown in Fig. 5. Features that

were seen in absorption in cooler models that lack hot stratospheres are now seen in emission. The planet is also brighter at every wavelength in the infrared. This would make the planet easier to detect with *Spitzer*. In addition, the models with hot stratospheres show limb brightening, rather than darkening.

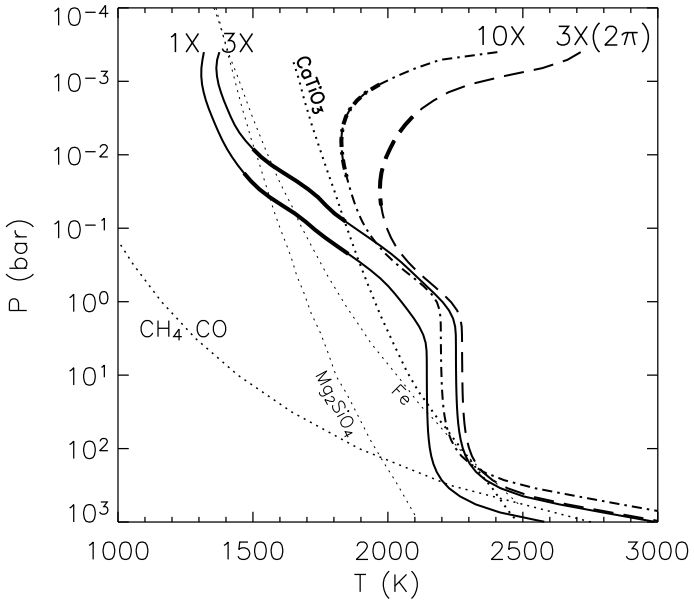

Figure 4. *Various P–T profiles for HD 149026b. These profiles assume metallicities of [M/H]=0.0 (labeled "1×"), [M/H]=0.5 (3×), and [M/H]=1.0 (10×) and assume efficient redistribution of absorbed stellar flux around the planet. Another [M/H]=0.5 profile is for the planet's day side only, and has the additional label "2π." The thick regions of the profiles show the pressures range from which the 3-30 μm spectra are generated. Condensation curves for the [M/H]=0.0 case are shown.*

4. Conclusions

We are now in a new age in the study of the atmospheres of Pegasi planets. This field will be driven by data from the *Spitzer Space Telescope* and other platforms such at the MOST telescope and groundbased infrared observations. The previous generation of atmospheres models were relatively simple and did not deviate from solar metallicity or equilibrium chemistry. The current generation is now beginning to ex-

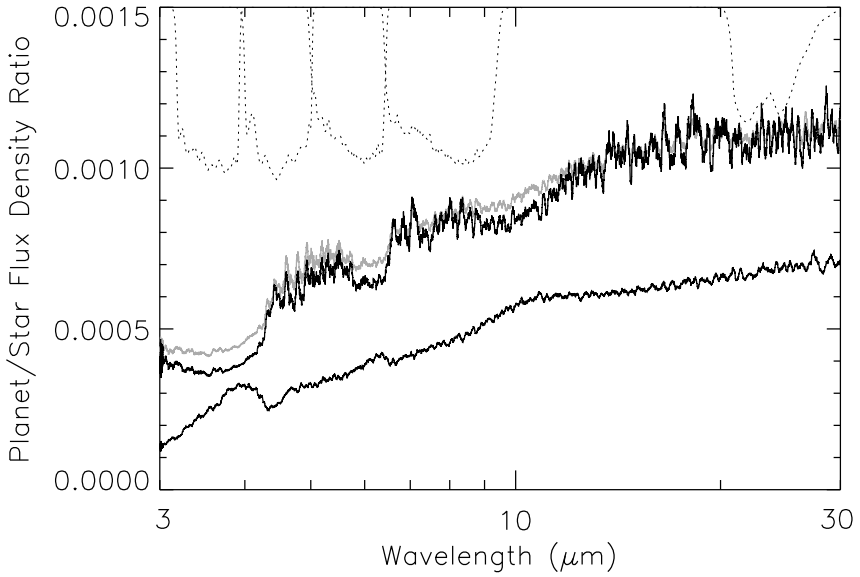

Figure 5. *Planet-to-star flux density ratios for HD 149026b. The three curves are for the 3× solar case (lower black), the 10× solar case (upper black), and the 3× solar day-side case (gray). Spitzer IRAC and MIPS bands are shown as dotted lines at the top.*

pand the model parameter space and does an adequate job of matching the available data. When matched against new observations, the next generation may have to incorporate new abundances, non-equilibrium chemistry, and atmospheric dynamics.

Acknowledgements. We acknowledge support from an National Research Council postdoctoral fellowship (JJF), NASA grants NAG2-6007 and NAG5-8919 (MSM), and NSF grant AST-0406963 (KL). This work was supported in part by the US Department of Energy under contract W-7405-ENG-36.

References

Ackerman, A. S. & Marley, M. S. 2001, ApJ, 556, 872
Barman, T. S., Hauschildt, P. H., & Allard, F. 2001, ApJ, 556, 885
Brown, T. M., Charbonneau, D., Gilliland, R. L. et al., 2001, ApJ, 552, 699
Burrows, A., Marley, M., Hubbard, W. B., et al, 1997, ApJ, 491, 856
Charbonneau, D., Allen, L. E., Megeath, et al., 2005, ApJ, 626, 523

Deming, D., Seager, S., Richardson, L. J., & Harrington, J. 2005, Nature, 434, 740

Fegley, B. J. & Lodders, K. 1994, Icarus, 110, 117

Fortney, J. J., Marley, M. S., Lodders, K. et al., 2005a, ApJL, 627, L69

Fortney, J. J., Saumon, D., Marley, M. S. et al., 2005b, astro-ph 0507422, subm. to ApJ

Iro, N., Bezard, B., & Guillot, T. 2005, A&A, 436, 719

Kurucz, R. 1993, CD-ROM 13, ATLAS9 Stellar Atmosphere Programs and 2 km/s Grid (Cambridge:SAO)

Lodders, K. 2002, ApJ, 577, 974

Lodders, K., 2003, ApJ, 591, 1220

Lodders, K. & Fegley, B. 2002, Icarus, 155, 393

Marley, M. S., Gelino, C., Stephens, D. et al., R. 1999, ApJ, 513, 879

Marley, M. S. & McKay, C. P. 1999, Icarus, 138, 268

Marley, M. S., Saumon, D., Guillot, T. et al., 1996, Science, 272, 1919

Marley, M. S., Seager, S., Saumon, D. et al, 2002, ApJ, 568, 335

Mayor, M. & Queloz, D. 1995, Nature, 378, 355

McKay, C. P., Pollack, J. B., & Courtin, R. 1989, Icarus, 80, 23

Richardson, L. J., Deming, D., & Seager, S. 2003, ApJ, 597, 581

Roellig, T. L., et al. 2004, ApJS, 154, 418

Sato, B., et al. 2005, ApJ, in press (astro-ph/0507009)

Seager, S. & Sasselov, D. D. 1998, ApJL, 502, L157

Sozzetti, A., et al. 2004, ApJL, 616, L167

Sudarsky, D., Burrows, A., & Hubeny, I. 2003, ApJ, 588, 1121

Tenth anniversary of 51 Peg-b : Status of and prospects for hot Jupiter studies
Proceedings of Haute Provence Observatory Colloquium (22-25 August 2005)
Edited by L. Arnold, F. Bouchy, and C. Moutou

Atmospheric dynamics of Pegasi planets

A. P. Showman and C. S. Cooper

Department of Planetary Sciences, Lunar and Planetary Laboratory, University of Arizona, Tucson, AZ 85721
[showman@lpl.arizona.edu]

Abstract. We present three-dimensional numerical simulations of the atmospheric dynamics of close-orbiting planets such as HD209458b. Our simulations show that winds of several $\mathrm{km\,sec^{-1}}$ and day-night temperature differences reaching 500 to 1000 K are possible at and above the photosphere. The circulation takes the form of a broad superrotating (eastward) equatorial jet. At $\sim$0.1 to 1 bar, the superrotation blows the hottest regions of the atmosphere downwind by $\sim 60^\circ$ of longitude, but at lower pressures the temperature pattern tracks the stellar illumination. We predict factors of several variation in the infrared flux received at Earth throughout an orbital cycle; if the photosphere is deep enough ($\geq$50 to 100 mbar pressure), the peak infrared emission should lead the time of secondary eclipse by 10 hours or more. Dynamics plays a key role in shaping the spectrum, clouds, chemistry, and long-term planetary evolution.

The past few years have witnessed many observations constraining the physical properties of extrasolar giant planets with orbital radii less than 0.1 AU (the "Pegasi planets" or hot Jupiters). Eight such planets have been discovered to undergo transits. Two such planets, HD209458b and TrES-1, have also been detected in thermal emission during the secondary eclipse, and several useful upper limits on composition, albedo, and thermal emission at various wavelengths have been achieved. This trend of detections is likely to continue.

A knowledge of atmospheric dynamics will be crucial for understanding these new observations. First, the interaction of dynamics with radiative transfer controls the temperature structure, which shapes the infrared spectrum and lightcurve. Most current radiative-transfer models adopt radiative-equilibrium conditions and make arbitrary assumptions about whether the absorbed stellar flux gets redistributed

across the planet or heats only the dayside; however, dynamics can push the atmosphere far from radiative equilibrium, and the extent of heat redistribution must be calculated explicitly (and may depend strongly on height). Second, whether clouds exist depends on the temperatures and locations of ascent/descent, which is again controlled by the circulation. Cloudiness in turn determines the albedo, visible lightcurves, and — if high-altitude clouds form — causes masking of spectral lines. Third, circulation may lead to disequilibrium between CO and CH_4, remove condensable species (Na_2S, $CaTiO_3$) via nightside cold trapping, and cause other chemical effects. Fourth, the atmospheric heat engine produces enormous kinetic energy, which, if transported deep enough, may affect the interior evolution. This has been suggested as a possible mechanism for producing the large radius of HD209458b, for example (Guillot & Showman 2002, Showman & Guillot 2002).

The intense starlight incident upon the surface of Pegasi planets leads to a deep radiative zone extending from the top of the atmosphere to pressures of ~ 1000 bars (e.g., Guillot et al. 1996, Guillot & Showman 2002, Burrows et al. 2003, Chabrier et al. 2004), and any observable weather occurs in this radiative zone. The fast spindown times for Pegasi planets implies that these planets should be in near-synchronous rotation (3.5 days for HD209458b)(Guillot et al. 1996, Showman & Guillot 2002). This rotation rate implies that rotation is important but not dominating: for km $\sec^{-1}$ winds, the Rossby number is ~ 1. These estimates imply dynamical length scales (the Rossby deformation radius and Rhines length) of order a planetary radius. As a result, any jets and gyres that exist should be global in scale. This contrasts with the case of Jupiter, where these length scales are only 2 to 10% of the planetary radius and — as a result — the dominant jets and vortices are much smaller than a planetary radius. Pegasi planets should therefore have physical appearances that differ greatly from Jupiter and Saturn.

Here we describe our recent work on the atmospheric circulation of Pegasi planets; the presentation describes and extends Cooper & Showman (2005), to which we refer the reader for details. We performed global, three-dimensional numerical fluid simulations using the ARIES/GEOS dynamical core (Suarez & Takacs 1995) in a domain extending from 1 mbar to 3 kbar. The simulations adopted the primitive equations, which are a simplified form of the Navier-Stokes equations valid for statically stable atmospheres that are vertically thin compared to their horizontal extent. We used parameters for HD209458b and assumed that the planetary interior is in synchronous rotation with the orbital period. The nominal resolution is 72×45 in longitude and latitude with 40 vertical levels. In the simulations, the dynamics are driven solely by the imposed day-night heating contrast. Rather than solving the radiative transfer explicity, we adopted a thermodynamic

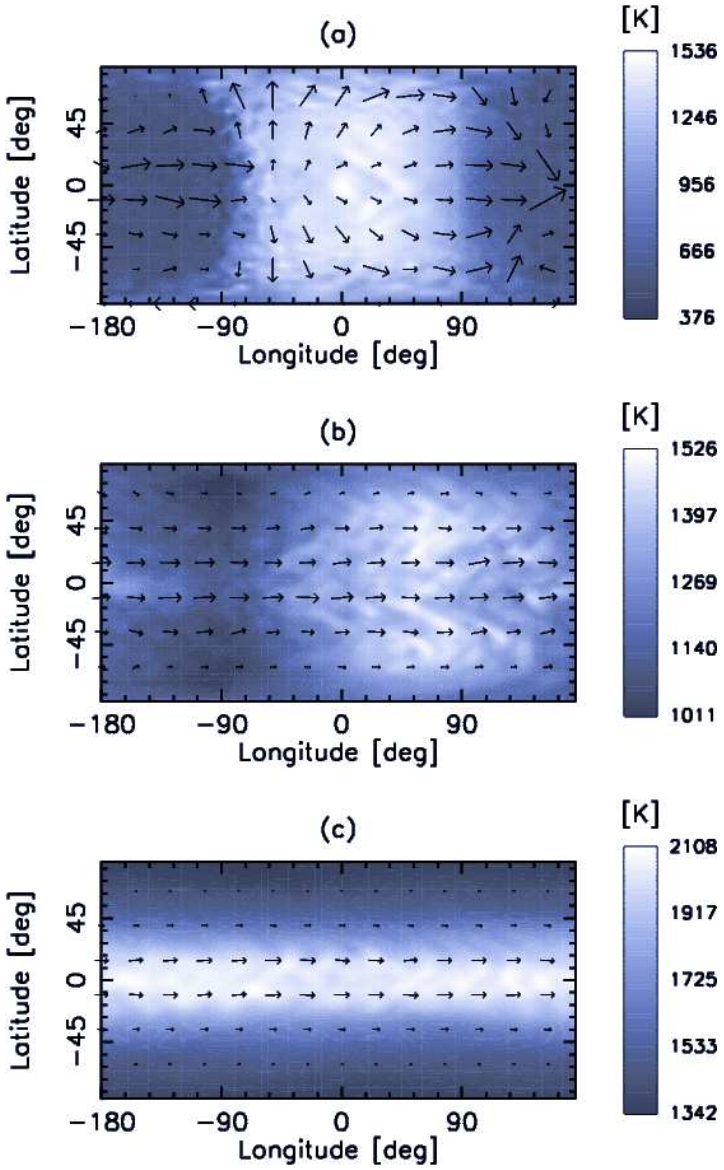

Figure 1. *Temperature (greyscale) and winds (arrows) at pressures of 2 mbar, 220 mbar, and 20 bars at 5000 Earth days of simulated time. Peak winds are 9.2, 4.1, and* $2.8\,\mathrm{km\,sec^{-1}}$ *from top to bottom, respectively. Heating occurs on the dayside (longitudes* $-90°$ *to* $90°$*) and cooling occurs on the nightside (longitudes* $-180°$ *to* $-90°$ *and* $90°$ *to* $180°$*). The substellar point is at* $0°$ *latitude,* $0°$ *longitude.*

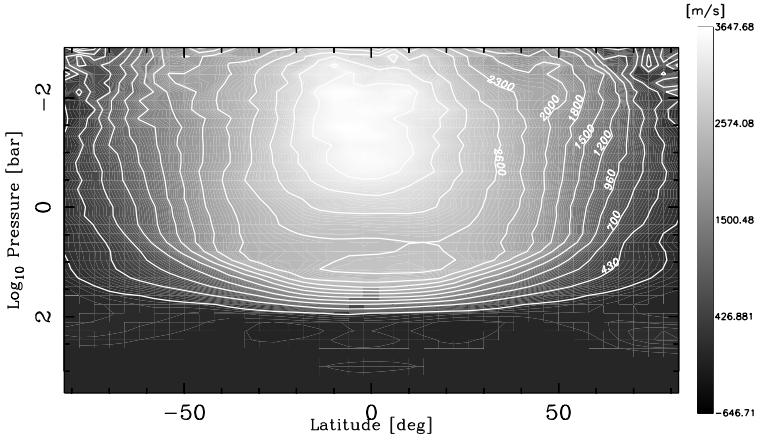

Figure 2. *Longitudinally averaged east-west winds versus latitude and pressure from the simulation in Figure 1. Positive values are eastward.*

heating rate (in $\mathrm{K\,sec^{-1}}$) of $(T_{\rm eq} - T)/\tau_{\rm rad}$, where $T_{\rm eq}$ is the specified radiative-equilibrium temperature profile (hot on the dayside and cold on the nightside), T is the actual temperature, and $\tau_{\rm rad}$ is the radiative-equilibrium timescale (a function of pressure). The vertical structure of $T_{\rm eq}$ and $\tau_{\rm rad}$ were taken from Iro et al. (2005); the day-night difference in $T_{\rm eq}$ was a free parameter that we varied from 100 to 1000 K.

Figure 1 shows the temperature (greyscale) and winds (arrows) for three layers (2 mbar, 200 mbar, and 20 bars from top to bottom, respectively) after a simulated time of 5000 Earth days. The imposed heating contrast leads to winds exceeding several $\mathrm{km\,sec^{-1}}$. By 5000 days the simulation has approximately reached a statistical steady state at pressures less than 3 bars, although the winds continue to increase at deeper levels. At the top (2 mbar), the radiative time constant is $\sim$ 1 hour (much less than the advection time), so the hot regions remain confined to the dayside. The temperatures are in near-radiative-equilibrium, with day-night temperature differences of $\sim 1000\,\mathrm{K}$. At 200 mbar, close to the expected photosphere if the planet lacks high-altitude clouds, a broad $\sim 4\,\mathrm{km\,sec^{-1}}$ eastward superrotation develops. Here, the radiative time constant, $\sim 10^5$ sec, is comparable to the time needed to advect air across a planetary radius. The circulation therefore blows the hottest regions of the atmosphere downwind from the substellar point by $\sim 60^\circ$ degrees of longitude. Temperature differences reach $\sim 500\,\mathrm{K}$ at this level.

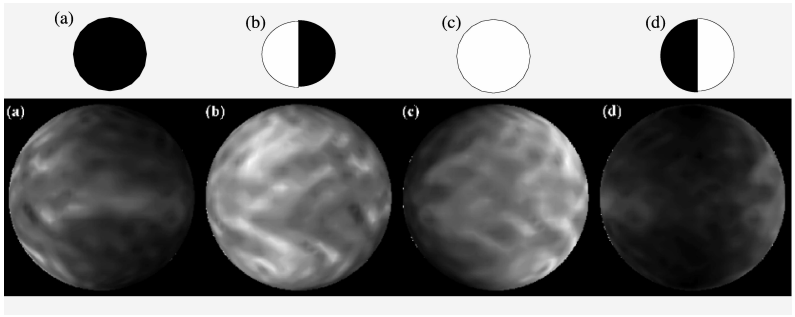

Figure 3. *Infrared brightness of HD209458b as viewed at Earth during (a) transit, (b) one-quarter period after transit, (c) secondary eclipse, and (d) one-quarter period after secondary eclipse. The planetary rotation axes are vertical, with the superrotating jet seen in Figure 1 going from left to right in each panel. The smaller schematic globes in the top row illustrate the illumination of the planet by sunlight, as viewed at Earth, during these same phases. Time increases from left to right.*

The development of a broad, superrotating (eastward) jet, with large day-night temperature differences at $p < 1$ bar, is a robust feature in all our simulations. We performed a variety of simulations using radiative-equilibrium temperature profiles from Burrows et al. (2003), Chabrier et al. (2004), or Iro et al. (2005); and using radiative-equilibrium day-night temperature differences of 1000, 750, 500, 250, or 100 K. We even performed simulations whose initial condition contained a broad *westward* equatorial jet extending from ~ 2 bars to the top of the domain. All of these simulations developed strong eastward jets resembling that in Figure 1. Furthermore, these results agree with Showman & Guillot (2002), who also obtained broad eastward jets in every one of their simulations using a different numerical code. This gives us confidence that eastward flow is a robust result, at least within the context of our adopted input parameters. What all these simulations have in common are short radiative time constants at pressures ≤ 1 bar, which allow the development of longitudinal temperature variations that are essentially a large-amplitude thermal tide. We speculate that, as has been suggested for Venus, this tide induces the superrotation by pumping eddy energy and eastward momentum upward and equatorward. (In absence of such eddy effects, the equatorial flow would be westward.)

Our results differ from the one-layer shallow-water calculations of Cho et al. (2003), which produce westward equatorial flow. However,

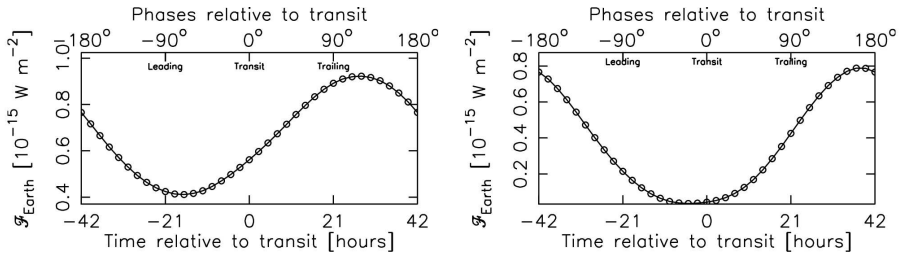

Figure 4. *Predicted infrared lightcurve for HD209458b assuming blackbody emission from the 220 mbar level (left) or the 10 mbar level (right).*

shallow-water turbulence invariably produces westward flow even for planets such as Jupiter and Saturn whose equatorial jets are eastward (e.g., Cho & Polvani 1996, Iacono et al. 1999; see Vasavada & Showman 2005 for a review). This feature seems to result from the exclusion of three-dimensional processes in the shallow-water equations.

The patterns in Figure 1 have implications for the infrared lightcurve of the planet throughout its orbit, as shown in Figures 3 and 4. The globes in Figure 3 (bottom row) show the infrared brightness at four phases assuming the planet emits as a blackbody from the 220 mbar level. The globes in the top row show the illumination as viewed from Earth during these same phases. The key point is that, in the absence of winds, the temperature pattern would follow the illumination (i.e., the infrared appearance would also correspond to the top row of globes). The differences between the idealized illumination patterns and the simulated brightness patterns result solely from atmospheric dynamics.

Figure 4 (left) shows the corresponding lightcurve assuming the photosphere is at the 220 mbar level, as might be expected for a cloud-free planet. Because the hot regions become offset from the substellar point at this pressure, the model predicts that the planet will radiate its maximum infrared flux toward Earth $\sim$ 14 hours *before* the secondary eclipse (rather than immediately around the time of secondary eclipse as would occur without winds). This effect could allow an observational determination of wind direction — if the winds are eastward, the peak fluxes would lead the eclipse, whereas if the winds are westward, peak fluxes would lag the eclipse.

Nevertheless, uncertainties exist regarding the emission level. The lower-than-expected Na (Charbonneau et al. 2002) and null detection of CO (Deming et al. 2005, Richardson et al. 2003) on HD209458b

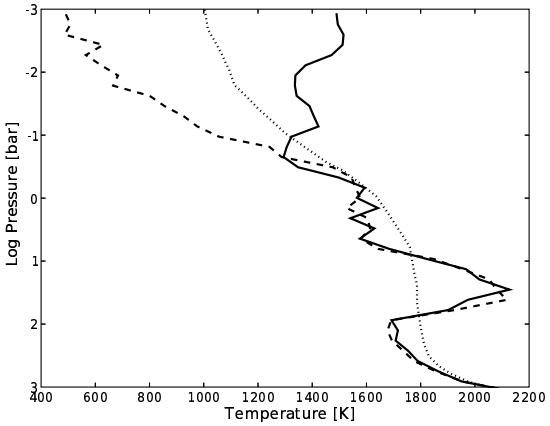

Figure 5. *Solid and dashed curves show the temperature profile at the substellar and antistellar points, respectively, for the simulation in Figure 1. The dotted line shows the globally averaged radiative-equilibrium profile from Iro et al. (2005). Note the formation of a dayside inversion layer at pressures less than 0.3 bars even though none exists in radiative equilibrium.*

could result from a high-altitude cloud at a few mbar pressure. If the cloud optical depth exceeds unity, then the primary infrared emission to space occurs from the cloud altitude rather than from the deeper levels expected for a cloud-free planet. Figure 4 (right) shows the lightcurve for the case of emission from the 10-mbar level. Because the radiative time constant is short at these pressures (Iro et al. 2005), the offset shown in Figure 4 (left) has largely disappeared. The magnitude of the flux differences has increased from $\sim$ two-fold (Figure 4, left) to eightfold (Figure 4, right). Emission from such high altitudes would largely mask the signature of winds. It is possible that some planets have high-altitude clouds while others do not (HD209458b and TrES-1 may represent these cases; Fortney et al. 2005), so a range of infrared-lightcurve behaviors is to be expected among real planets.

Dynamics can push the atmosphere far from radiative equilibrium, and this may have implications in explaining the existing Spitzer IRAC data at 4.5 and 8 μm for TrES-1 (Charbonneau et al. 2005). Current radiative-equilibrium models cannot easily explain the data: if they explain the 4.5 μm flux, then they do not predict enough flux at 8 μm (Fortney et al. 2005, Burrows et al. 2005, Seager et al. 2005, Barman

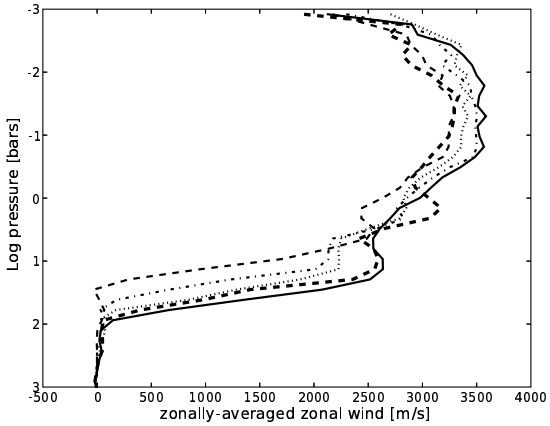

Figure 6. *Time evolution of the longitudinally averaged equatorial east-west winds from the simulation in Figure 1. Thin dashed, dash-dot, dotted, thick dashed, and solid curves show profiles at 1000, 2000, 3000, 4000, and 5000 Earth days of simulated time. Note the gradual downward penetration of winds from 10 to 100 bars over the course of the simulation.*

et al. 2005). Part of the problem is that 8-μm photons are emitted from higher altitude, where radiative-equilibrium models predict colder temperatures. One solution is to invoke a temperature inversion so that the emission region for 8-μm photons is hotter than for 4.5-μm photons. Fortney et al. (2005) accomplished this by adding an *ad hoc* heat source, which lead to an improved fit to the Spitzer data. A key point is that dynamics can *naturally* produce such a dayside temperature inversion, even when no such inversion would exist in radiative equilibrium (Figure 5). The inversion occurs because of the upward-decreasing radiative time constant: as air columns superrotate from nightside to dayside, the air at the top warms much more rapidly than air at the bottom, producing an inversion. No *ad hoc* heat sources need be invoked.

The large radius of HD209458b has remained a puzzle, particularly given that the other 7 known transiting planets have radii in agreement with evolution calculations (e.g., Guillot 2005). Showman & Guillot (2002) and Guillot & Showman (2002) suggested that mechanical energy produced by the atmospheric heat engine could be advected into the interior, where it could be dissipated and might provide a source of

heat that would slow the contraction. In the current simulations, all of the heating/cooling (which is the sole energy source in the simulations) occurs at pressures ≤ 10 bars. Nevertheless, the simulations gradually develop strong winds at pressures > 10 bars, which implies that kinetic energy is transported downward from the heated regions into the interior. Figure 6 shows the evolution of longitudinally averaged winds at the equator over time. The winds at pressures ≤ 1 bar rapidly reach a quasi-steady equilibrium, but the winds from 10 to 100 bars increase throughout the simulation (this implies a large increase in total kinetic energy because that layer contains ten times more mass than the entire overlying atmosphere). The build-up of winds in Figure 5 corresponds to a downward kinetic energy flux of $\sim 10^3\,\mathrm{W\,m^{-2}}$, which is 10 to 100 times greater than the intrinsic flux predicted in evolution models (e.g., Guillot & Showman 2002, Burrows et al. 2003, Chabrier et al. 2004). More work is needed to determine the fate of this energy, but it suggests that atmospheric circulation could affect the long-term evolution.

Acknowledgements. This work was supported by NSF grant AST-0307664 and NASA GSRP NGT5-50462.

References

Barman, T.S., Hauschildt, P.H., & Allard, F. 2005, ApJ, in press

Burrows, A., Sudarsky, D., & Hubbard, W.B. 2003, ApJ, 594, 545

Burrows, A., Hubeny, I., and Sudarsky, D. 2005, ApJ, 625, L135

Chabrier, G., Barman, T., Baraffe, I., *et al.*, 2004, ApJ, 603, L53

Charbonneau, D., Brown, T.M., Noyes, R.W., & Gilliland, R.L. 2002, ApJ, 568, 377

Charbonneau, D. et al. 2005, ApJ, 626, 523

Cho, J.Y-K., & Polvani, L.M. 1996, *Science*, 273, 335

Cho, J.Y-K., Menou, K., Hansen, B.M.S., & Seager, S. 2003, ApJ, 587, L117

Cooper, C.S., & Showman, A.P. 2005, ApJ, 629, L45

Deming, D., Brown, T.M., Charbonneau, D., *et al.*, 2005, ApJ, 622, 1149

Fortney, J.J., Marley, M.S., Lodders, K., *et al.*, 2005, ApJ, 627, L69

Guillot, T., Burrows, A., Hubbard, W.B., *et al.*, 1996, ApJ, 459, L35

Guillot, T., & Showman, A.P. 2002, A&A, 385, 156

Guillot, T. 2005, *Ann. Rev. Earth Planet. Sci.*, 33, 493

Iacono, R., Stuglia, M.V., & Ronchi, C. 1999, *Phys. Fluids*, 11, 1272

Iro, N., Bézard, B., & Guillot, T. 2005, A&A, 436, 719

Richardson, L.J., Deming, D., & Seager, S. 2003, ApJ, 597, 581

Seager, S., Richardson, L.J., Hansen, B.M.S., *et al.*, 2005, ApJ, submitted

Showman, A.P., & Guillot, T. 2002, A&A, 385, 166

Vasavada, A.R., & Showman, A.P. 2005, *Rep. Prog. Phys.*, 68, 1935

Tenth anniversary of 51 Peg-b : Status of and prospects for hot Jupiter studies
Proceedings of Haute Provence Observatory Colloquium (22-25 August 2005)
Edited by L. Arnold, F. Bouchy, and C. Moutou

Search for exospheric signatures from the atmosphere of HD209458b

N. Iro[1,2], A. Coustenis[1], C. Moutou[3], M. Mayor[4], and D. Queloz[4]

[1]*LESIA – Observatoire de Paris-Meudon, FRANCE*
[nicolas.iro@obspm.fr]

[2]*Department of Physics – University of Florida, USA*

[3]*LAM – Marseille, FRANCE*

[3]*Observatoire de Genève, SWITZERLAND*

Abstract.
Observations at the VLT with UVES in 2002 during 6 transits give access to spectral regions where signatures from the atmosphere of HD209458b may appear. We observe ON- and OFF-transit spectra and check the differences for new absorption features. We present in this paper a tentative search in the spectral regions where features of sodium or H_2O^+ can be present.

1. Introduction

HD209458b, the first discovered extrasolar planet transiting its star, has been subject to several studies constraining the composition of its atmosphere, in particular Na (Charbonneau et al. 2002 ; Narita et al. 2005), HeI (Moutou et al. 2003), CO (Deming et al. 2005) , H (Bundy & Marcy 2000 ; Vidal-Madjar et al. 2003 ; Vidal-Madjar et al. 2004 ; Winn et al. 2004 ; Narita et al. 2005), O, C and Si (Vidal-Madjar et al. 2004), Ca (Bundy & Marcy 2000 ; Narita et al. 2005 ; Shkolnik et al. 2005) and Fe (Bundy & Marcy 2000 ; Narita et al. 2005).

We performed observations with UVES in the 0.33-0.67 μm region at high spectral resolution. We searched for ions and neutral molecules originating in the planet's exosphere and located in the evaporated material around the planet, occulting its primary star (Coustenis et al.

1997). Iro et al. (2004) presented the planet-induced chromospheric activity on HD209458 in these data as well as the He feature at 1.083 μm with data from VLT/ISAAC (Moutou et al. 2003). In this paper, we focus on the search for features from Na and H_2O^+.

2. The 2002 UVES campaign

We used VLT/UVES to observe HD209458 in 2002 over 6 of its transits, thus accumulating the time required to obtain a S/B of about 1000, required in order to detect a possible evaporated exosphere. The observations were spread out between June and September 2002. An equivalent time of observation was dedicated to the observation of the system off-transit, to supply a spectrum of comparison of the primary star equivalent to the on-transit spectrum. Finally, a particular effort was devoted to the calibration of the event, at the same time by inserting frequent observations of a comparison star so as to insure the determination of the telluric contribution, and to provide a high-quality calibration of the instrument.

The data are in the course of analysis since the beginning of 2003. The production of a spectrum of transmission with no telluric or stellar contamination requires a meticulous reduction which we perform ourselves. We note the excellent quality of the majority of the spectra.

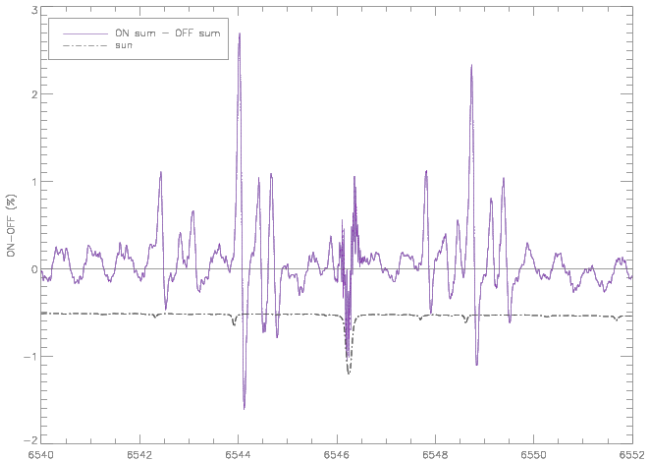

Figure 1. *Difference between the sum of all the OFF-transit spectra and the sum of all the ON-transit spectra. The solar spectrum is shown in arbitrary units. We find a strong dissymmetry between ON and OFF at the H_2O^+ line position at 6544 Å.*

3. Data analysis

We averaged the spectra for all the transits in order to obtain ON-transit and OFF-transit spectra with a better S/N ratio. We then calculate the difference between the ON- and the OFF-spectra for the spectral ranges of interests. We performed this analysis for the Na line doublet at 5891.9 and 5893.2 Åwhere we note a dissymetry between the On- and the OFF- transit spectra. We also remarked dissymmetric features in the region of H_2O^+ lines at 6544 (see Fig. 1) and 6193 Å (the nominal position of the H_2O^+ line is 6198 Å).

4. Perspectives

The spectral ranges contained in the data presented in this paper include positions of possible features from Hα (6563 Å) and Hβ (4861 Å), Fe (6024 Å), O I (5577 and 6364 Å), CO^+ (4911 and 5490 Å). The analysis of these spectral regions are in progress.

References

Bundy, k. A. & Marcy, G. W. 2000, PASP, 112, 1421

Charbonneau, D., Brown, T. M., Noyes, R. W., et al. 2002, ApJ, 568, 377

Coustenis, A., Scheider, J., Wittemberg, R., et al. 1997. ASP 134, 296-303

Deming, D., Brown, T. M., Charbonneau, D., et al. 2005, ApJ, 622, 1149

Iro, N., Coustenis, A., Moutou, C., et al. 2004 in ASP Conf. Ser. Vol. 321, Extrasolar Planets: Today and Tomorrow, 209

Moutou, C., Coustenis, A., Schneider, J., et al. 2003. A & A 405, 341.

Narita, N. ,Suto, Y.,Winn, J. N., et al. 2005, PASJ, 57, 471

Shkolnik, E., Walker, G. A. H., Bohlender, D. A., et al. 2005, ApJ, 622, 1075

Vidal-Madjar, A., Lecavelier des Etangs, A., Désert, J.-M., et al. 2003, Nature, 422, 143

Vidal-Madjar, A., Désert, J.-M., Lecavelier des Etangs, A., et al. 2004, ApJL, 604, L69

Winn, J. N., Suto, Y., Turner, E. L., et al. 2004, PASJ, 56, 655

Tenth anniversary of 51 Peg-b : Status of and prospects for hot Jupiter studies
Proceedings of Haute Provence Observatory Colloquium (22-25 August 2005)
Edited by L. Arnold, F. Bouchy, and C. Moutou

Subaru HDS transmission spectroscopy of the transiting extrasolar planet HD 209458b

N. Narita[1], Y. Suto[1], J. N. Winn[2], E. L. Turner[1,3], W. Aoki[4], C. J. Leigh[5], B. Sato[4], M. Tamura[4], and T. Yamada[4]

[1]*Department of Physics, School of Science, The University of Tokyo, Tokyo, 113-0033, Japan [narita@utap.phys.s.u-tokyo.ac.jp]*

[2]*Harvard-Smithsonian Center for Astrophysics, 60 Garden St. MS-51, Cambridge, MA 02138, USA*

[3]*Princeton University Observatory, Peyton Hall, Princeton, NJ 08544, USA*

[4]*National Astronomical Observatory of Japan, Tokyo, 181-8588, Japan*

[5]*Liverpool John Moore's University, Astrophysics Research Institute, Birkenhead, CH41, 1LD, U.K.*

Abstract. We have searched for absorption in several common atomic species due to the atmosphere or exosphere of the transiting extrasolar planet HD 209458b, using high precision optical spectra obtained with the Subaru High Dispersion Spectrograph (HDS). Previously we reported an upper limit on Hα absorption of 0.1% (3σ) within a 5.1Å band. Using the same procedure, we now report upper limits on absorption due to the optical transitions of Na D, Li, Hα, Hβ, Hγ, Fe, and Ca. The 3σ upper limit for each transition is approximately 1% within a 0.3Å band (the core of the line), and a few tenths of a per cent within a 2Å band (the full line width). The wide-band results are close to the expected limit due to photon-counting (Poisson) statistics, although in the narrow-band case we have encountered unexplained systematic errors at a few times the Poisson level. These results are consistent with all previously reported detections (Charbonneau et al. 2002) and upper limits (Bundy & Marcy 2000; Moutou et al. 2001), but are significantly more sensitive yet achieved from ground based observations.

1. Observations and Reduction Method

We observed HD 209458 on the nights of HST 2002 October 24 and 26 (25 and 27 in UT) with the Subaru HDS, We obtained 30 spectra of HD 209458, covering 4100Å $< \lambda <$ 6800Å with a spectral resolution of $R \approx 45000$ (0.9 km s^{-1} per pixel). Compared with the previous investigations, the HDS data cover a larger range of wavelengths (covering the entire optical band) and have a higher signal-to-noise ratio. Moreover, this data set has a substantial advantage of covering a wide range of orbital phases, namely before, during and after the transit in a single night. First, we processed the frames with standard IRAF procedures and extracted one-dimensional spectra. Next, we applied an analysis method described at length in Winn et al. (2004) to correct for substantial time-dependent variations of the instrumental blaze function. Next, a template spectrum $T(\lambda)$ is created from all 30 individual exposures using the above correction method. A time series of residual spectra are generated by subtracting the suitably matched template $T_{\rm m}(\lambda)$ from each spectrum $S(\lambda, t)$. Then we compute a time series of fractional difference in flux between the spectrum and the matched template within a smoothing width $\Delta\lambda$ according to

$$\delta_{\rm A}(t) = \frac{\displaystyle\int_{\lambda_0-\Delta\lambda/2}^{\lambda_0+\Delta\lambda/2} d\lambda \quad [S(\lambda,t) - T_{\rm m}(\lambda)]}{\displaystyle\int_{\lambda_0-\Delta\lambda/2}^{\lambda_0+\Delta\lambda/2} d\lambda \;\; T_{\rm m}(\lambda)}, \tag{1}$$

where A indicates each target absorption line. To place a quantitative limit on additional absorption, we calculate $\bar{\delta}_{\rm in,A}$ and $\sigma_{\rm in,A}$:

$$\bar{\delta}_{\rm in,A} \equiv \frac{1}{N_{\rm in}} \sum_{t={\rm in}} \delta_{\rm A}(t)\,, \;\; \sigma_{\rm in,A} \equiv \sqrt{\frac{1}{N_{\rm in}} \sum_{t={\rm in}} \left[\bar{\delta}_{\rm in,A} - \delta_{\rm A}(t)\right]^2}\,, \tag{2}$$

which are the mean value and the standard deviation of $\delta_{\rm A}(t)$ for the spectra taken in the transit. Similarly, we compute $\bar{\delta}_{\rm out,A}$ and $\sigma_{\rm out,A}$ from the spectra taken out of the transit. The numbers of spectra in each phase are $N_{\rm in} = N_{\rm out} = 12$. Finally, we compute

$$\bar{\delta}_{\rm A} \equiv \bar{\delta}_{\rm in,A} - \bar{\delta}_{\rm out,A}\,, \;\; \sigma_{\rm A} \equiv \sqrt{\frac{N_{\rm in}\sigma_{\rm in,A}^2 + N_{\rm out}\sigma_{\rm out,A}^2}{N_{\rm in} + N_{\rm out}}} = \sqrt{\frac{\sigma_{\rm in,A}^2 + \sigma_{\rm out,A}^2}{2}}\,. \tag{3}$$

Note that $\bar{\delta}_{\rm A}$ would be negative if there were additional absorption during transit. Where no additional absorption feature related to transit are detected (i.e., $|\bar{\delta}_{\rm A}| < \sigma_{\rm A}$), we quote upper limits as $3\sigma_{\rm A}$.

2. Results

An investigation of the optical spectra taken during a transit of the HD 209458 system with Subaru HDS revealed no additional absorption features associated with the transit. The summary of our upper limits are shown in Table 1. The typical achieved sensitivity level is $\sim 1\%$ (3σ) for $\Delta\lambda = 0.3$Å (the line cores) in fractional difference spectra, and a few times smaller for $\Delta\lambda = 2$Å(the full line width). Although we cannot confirm the smaller level of absorption in the Na D line that was observed from space, our upper limits for the other optical transitions are consistent with, but more stringent than, those previously achieved from the ground. More details are given by Narita et al. (2005).

Table 1. *Summary of the 3σ upper limits.*

Element	λ_0 (Å)	$\Delta\lambda = 0.3$Å (%)	$\Delta\lambda = 2$Å (%)
red CCD			
Li I	6707.95	0.91	0.43
Hα	6562.95	0.81	0.66
Fe I	6024.20	0.84	0.18
Na I(D1)	5896.06	1.43	0.28
Na I(D2)	5890.09	0.85	0.18
Na I	5887–5899	0.12	(for 12Å)
blue CCD			
Hβ	4861.45	0.68	0.34
Fe I	4383.65	1.08	—
Hγ	4340.56	1.57	0.88
Ca I	4226.82	2.14	—

Acknowledgements. The visit of N.N. to OHP is supported by the scholarship for Ph.D. students from this conference and the University of Tokyo. I greatly appreciate LOC's very kind hospitality during my stay at OHP.

References

Bundy, K. A., & Marcy, G. W. 2000, PASP, 112, 1421
Moutou, C., Coustenis, A., Schneider, J., *et al.*, 2001, A&A, 371, 260
Charbonneau, D., Brown, T. M., Noyes, R. W., *et al.*, 2002, ApJ, 568, 377
Winn, J. N., Suto, Y., Turner, E. L., *et al.*, 2004, PASJ, 56, 655
Narita, N., Suto, Y., Winn, J. N., *et al.*, 2005, PASJ, 57, 471